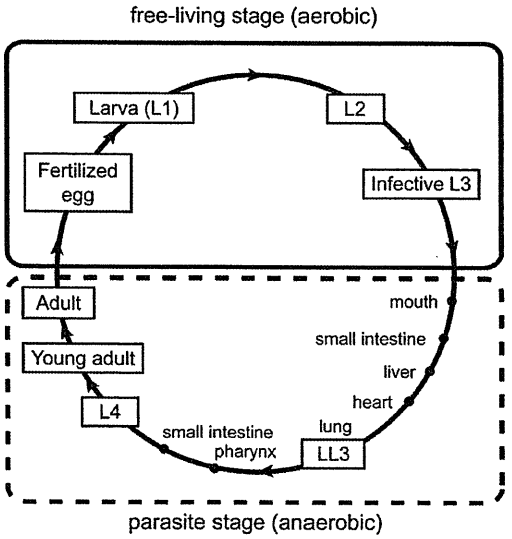

Fig. 1. Life cycle of *Ascaris suum*. Fertilized eggs embryonate and become infective third-stage larvae (L3) under normoxic conditions. L3 are ingested by the host and hatch in the small intestine. Afterwards, larvae migrate into the host organs (liver, heart, lung, pharynx), and finally reach the small intestine and develop into adult worms. In the small intestine, the oxygen concentration is lower than 5%.

(CybL), and the small (CybS) subunit, and functions as a succinate–ubiquinone reductase in the aerobic respiratory chain (Kita and Takamiya, 2002; Sakai et al., 2012). In a previous study, we showed that *A. suum* mitochondria express stage-specific isoforms of complex II (Amino et al., 2000, 2003; Saruta et al., 1995) and recently determined the structure of adult-type complex II (Shimizu et al., 2012). Fp and CybS subunits are distinct between the adult and larval forms, and expressions of these genes are controlled at the transcriptional level. However, the regulatory mechanisms responsible for the stage-specific expression of these genes have not been elucidated. Considering that *A. suum* does not have a respiratory or circulatory system, transcription factors are supposed to play important roles in sensing oxygen levels and induction of target genes.

In mammals, hypoxia-inducible factor-1 (HIF-1) is a key regulator of physiological responses to hypoxia. HIF-1 activates the transcription of numerous genes, including genes involved in erythropoiesis, angiogenesis, and glycolysis (Kaelin and Ratcliffe, 2008; Semenza, 2011). HIF-1 is a heterodimeric protein composed of HIF-1α and HIF-1β subunits, both of which are members of the bHLH-PAS (basic helix–loop–helix/Per-Arnt-Sim) family of transcription factors (Wang et al., 1995). The bHLH regions are known to be required for DNA binding and dimerization, and the PAS domains are suggested to be involved in dimerization, ligand binding, and other biological activities (Jiang et al., 1996; Zelzer et al., 1997). On the C-terminal side of the PAS domain, HIF-1α contains the oxygen-dependent degradation domain (ODD) and two transactivation domains, the N-terminal transactivation domain (N-TAD, spanning residues 531–575 of human HIF-1α) and the oxygen-regulated C-terminal transactivation domain (C-TAD, spanning residues 786–826 of human HIF-1α) (Jiang et al., 1997; Pugh et al., 1997). HIF-1β also possesses an activation domain named the C-terminal activation domain (CAD) (Jain et al., 1994).

Under normoxic conditions, HIF-1α is targeted for polyubiquitination and proteosomal degradation through the oxygen-dependent hydroxylation of the conserved proline residues in the ODD by HIF prolyl hydroxylases (PHDs) and interaction with the von Hippel–Lindau tumor suppressor protein (VHL) (Epstein et al., 2001; Ivan et al., 2001; Jaakkola et al., 2001). The transcriptional activity of HIF-1α is also regulated by hydroxylation of the conserved asparagine residue in its C-TAD by factor inhibiting HIF (FIH) (Lando et al., 2002a,b). In contrast, prolyl hydroxylation and subsequent degradation of HIF-1α is inhibited under hypoxia. This permits HIF-1α to translocate to the nucleus, dimerize with HIF-1β, and activate the expression of target genes, which act to increase oxygen delivery or implement metabolic adaptation (Kallio et al., 1998).

HIF-1 homologs have been identified and characterized in a diverse array of multicellular organisms, and its function is also required for hypoxic adaptation in the free-living nematode, *Caenorhabditis elegans* (Jiang et al., 2001a; Powell-Coffman et al., 1998). The ubiquitous presence and diverse functions of HIF-1 suggest that it also plays crucial roles in hypoxic adaptation in *A. suum*.

In the present study, cDNAs for HIF-1α and HIF-1β homologs of *A. suum* were cloned by RT-PCR using degenerate primers. The functional interaction between *A. suum* HIF-1α and HIF-1β was confirmed by yeast two-hybrid assays. Furthermore, *hif-1* mRNA expression levels were examined in the aerobic free-living stages (fertilized eggs, L3 larvae) and the anaerobic parasitic stages (LL3, young adult worms, and adult muscle tissue). In addition, nucleotide sequences of 5′-upstream regions of complex II genes were determined and searched for hypoxia-responsive elements (HREs).

2. Material and methods

2.1. Experimental animals

Adult *A. suum* worms were collected from the intestines of infected pigs in a slaughterhouse in Tokyo, Japan. Adult worms were dissected to obtain muscle and uterine tissue. Fertilized eggs were isolated from uterine tissue of adult worms, which had been stored in 0.5 M sodium hydroxide at 4 °C, by homogenization and centrifugation and allowed to develop to L3 aerobically as previously described (Iwata et al., 2008). For preparation of LL3 larvae and young adult worms, pigs were orally infected with eggs containing L3 larvae (approximately 10^5 and 10^4 eggs per pig, respectively), and worms were collected from the lungs and small intestine of the pig 7 days and 38 days after ingestion, respectively (Islam et al., 2006). This study was carried out in strict accordance with the recommendations of the Guide for the Care and Use of Laboratory Animals of the National Institutes of Animal Health. The protocol was approved by the Committee of the Ethics of Animal Experiments of the NIAH (Permit Number: 07-29, 08-023, 09-019, 10-007). All surgeries were performed under sodium pentobarbital anesthesia, and all efforts were made to minimize the animals' suffering. Whole bodies of the *A. suum* worms were used for total RNAs extraction, except that muscle tissue, which comprises the most part of an adult worm, was used as the representative of a whole body of an adult worm to avoid the interfusion of eggs existing in female adult genital tracts. Each sample was immediately frozen with liquid nitrogen and stored at −80 °C until use.

2.2. Cloning of *A. suum hif-1α and hif-1β cDNAs*

Frozen muscle of an adult *A. suum* worm was pulverized in a mortar and pestle containing liquid nitrogen, and total RNAs were extracted by the acid guanidinium-phenol-chloroform (AGPC) method (Chomczynski and Sacchi, 1987). Poly(A)$^+$ RNAs were purified from total RNAs using an Oligo (dT)-Cellulose column (GE Healthcare). For the cloning of the partial sequences of *hif-1* cDNAs and the following 5′RACE, cDNA was synthesized with random primers $(N)_6$ (Takara) using ReverTraAce (Toyobo) as a reverse transcriptase. For the 3′ RACE, the oligo (dT) primer P-383 was used (Table 1).

Partial sequences corresponding to the bHLH and the PAS domains of nematode *hif-1α* were obtained by a TBLASTN search of the Nematode.net website (http://www.nematode.net/) and TIGR database (http://www.jcvi.org/) using the amino acid sequences of *C. elegans hif-1* (*C. elegans hif-1α*) (GenBank ID: NM_001028722) as a query. The degenerate primers were designed based on the conserved amino acid sequences

Table 1
Primers used in this study.

P-80	(F)	5′-GGTTTAATTACCCAAGTTTGAG-3′
P-383	(R)	5′-$(T)_{18}$ AAGGACGCCGGCGCTTAAGAAGGTCAA-3′
P-385	(R)	5′-GAATTCGCGGCCGCAG-3′
P-746	(F)	5′-GNATGGCNGTNTCNCA(C/T)ATG-3′
P-747	(R)	5′-A(A/G)(A/G)AANCCAT(C/T)NGC(A/C/T)GC(C/T)TC-3′
P-753	(F)	5′-CTATCCGTGGTACGTCTCAG-3′
P-754	(R)	5′-GTATTAGGTGCTTCAGTTCTTGG-3′
P-755	(R)	5′-CTGGAAGAATTCGCGGC-3′
P-758	(F)	5′-GACAGACCAAGAACTGAAGC-3′
P-759	(R)	5′-GAGACGTACCACGGATAGC-3′
P-1900	(F)	5′-CGCCATGGCAATGTCAAAGTATGCACGGAATG-3′
P-1904	(R)	5′-AAGGATCCTAACAAGACCGTCTTTGAG-3′
P-2086	(F)	5′-CC(T/A)ATTGTTGA(A/C/T)GAAG-3′
P-2087	(F)	5′-TA(C/T)(C/T)T(C/T/A)GGA(C/T)T(T/A)AC(A/G)CA(A/G)-3′
P-2090	(R)	5′-CAT(A/G)TC(G/A)(C/T)A(A/T/G)GT(A/G)TG-3′
P-2103	(R)	5′-ATC(T/G)GC(T/C)GGAT(G/A)(T/A)A(T/C)(T/C)AA-3′
P-2132	(R)	5′-CACAAATTCCTTCAGAGATCG-3′
P-2133	(F)	5′-CGTGGAAGAAATCTCAACCTC-3′
P-2134	(R)	5′-GAGGTTGAGATTTCTTCCACG-3′
P-2135	(F)	5′-CAAGAGTGCTGAAATCCCTAAC-3′
P-2582	(F)	5′-CGATCTCTGAAGGAATTTGTG-3′
P-2951	(F)	5′-CATCGAATTCATGATGGCCGATCATGGTGGTG-3′
P-2953	(R)	5′-GTCGCTGAGCTCCTATGCCGCCGAAGTATCTCTACG-3′

Abbreviations: F, forward; R, reverse; N, A, C, G, or T.
The underlined sequences indicate the restriction sites: CCATGG, *Nco*I; GGATCC, *Bam*HI; GAATTC, *Eco*RI; GAGCTC, *Sac*I.

among nematodes: *C. elegans*, *Brugia malayi* (TIGR database ID: 14615.m00142), and *Strongyloides ratti* (GenBank ID: CD523815). The nucleotide sequences and positions of the primers used for cloning of *A. suum hif-1α* and *hif-1β* are shown in Table 1 and Fig. 2, respectively. The first PCR was performed using a forward primer designed based on the spliced leader sequence 1 (SL1) of nematodes (Nilsen et al., 1989), P-80, and a reverse degenerate primer P-2103. The first PCR product was used as a template for the nested PCR with degenerate primers, P-2086 and P-2103. Further PCR amplification was carried out from the nested PCR product with degenerate primers, P-2087 and P-2090. PCR was performed under low stringent thermal conditions consisting of 30 cycles of 90 °C for 30 s, 42 °C for 1 min, 72 °C for 1 min. The resulting PCR product with the expected size (360 bp) was inserted into the pGEM-T plasmid (Promega) and sequenced. Specific primers for 5′ and 3′-RACE were designed from the nucleotide sequence of the subcloned fragment. For 5′-RACE, the first PCR was performed with SL1 primer P-80 and a specific primer P-2134. Nested PCR was carried out using P-80 and a specific primer P-2132. For 3′-RACE, the first PCR was carried out using a specific primer P-2133 and an adapter primer P-755. Nested PCR was carried out with a specific primer P-2135 and an adapter primer P-385.

For cloning of partial sequences of *hif-1β*, degenerate primers were designed based on the conserved amino acid residues corresponding to the bHLH regions of *hif-1β* of various organisms: *Homo sapiens* (GenBank ID: NM_001668), *Bos taurus* (GenBank ID: AB053954), *Rattus norvegicus* (GenBank ID: NM_012780), *Mus musculus* (GenBank ID: BC012870), *Gallus gallus* (GenBank ID: AF348088), *Xenopus laevis* (GenBank ID: AY036894), *Drosophila melanogaster* (GenBank ID: AF154417), and *C. elegans* (GenBank ID: AF039569). The PCR reaction was performed with 30 cycles of 94 °C for 45 s, 53 °C for 30 s, 72 °C for 90 s using degenerate primers P-746 and P-747. The PCR product with the expected size (130 bp) was cloned into the pGEM-T plasmid (Promega) and sequenced. 5′RACE was performed with SL1 primer P-80 and a specific primer P-754. Nested PCR was carried out using P-80 and a specific primer P-759. For 3′RACE, first PCR was carried out using specific primers P-753 and P-755. Nested PCR was carried out with specific primers P-758 and P-385.

2.3. Construction of the prey and bait plasmids for yeast two-hybrid assay

A. suum hif-1α and *hif-1β* cDNAs were fused to the GAL4 activation domain of the prey plasmid pGADT7 (Clontech) and the GAL4 DNA-binding domain of the bait plasmid pGBKT7 (Clontech), respectively. DNA fragments of *A. suum hif-1α* and *hif-1β* were amplified by PCR using *Pfu* turbo DNA polymerase (Stratagene) and pGEM-T (*hif-1α*) or pGEM-T (*hif-1β*) plasmid DNA as a template with primers in which restriction sites were incorporated. Primers P-2951 and P-2953 were used for *hif-1α* amplification, while primers P-1900 and P-1904 were used for *hif-1β* amplification. Nucleotide sequences of the primers are shown in Table 1.

PCR products were digested with the appropriate restriction enzymes and inserted into plasmids with T4 DNA ligase (Invitrogen).

2.4. Yeast two-hybrid assay

The interaction between recombinant *A. suum* HIF-1α and HIF-1β was analyzed by the yeast two-hybrid assay using MATCHMAKER GAL-4 Two-Hybrid Systems (Clontech) according to the manufacturer's instructions. The prey plasmid pGADT7-GAL4-HIF-1α expressing a fused protein of HIF-1α and the GAL4 activation domain, and the bait plasmid pGBKT7-GAL4-HIF-1β expressing a fused protein of HIF-1β and the GAL4 DNA binding domain, were introduced into competent AH109 yeast cells by the polyethylene glycol (PEG)/lithium acetate-based method. Transformants were plated on synthetic dropout (SD) agar plates lacking leucine/tryptophan or adenine/histidine/leucine/tryptophan and incubated at 30 °C until the appearance of colonies.

2.5. Real-time PCR

Transcript levels of *A. suum hif-1α* and *hif-1β* mRNAs at different developmental stages were determined by real-time PCR. Triplicate samples of fertilized eggs, L3, and adult muscle tissue, and single samples of LL3 and young adult worms were pulverized in a mortar and pestle containing liquid nitrogen, and total RNAs were extracted using Trizol LS Reagent (Invitrogen). Total RNAs of each sample were treated with

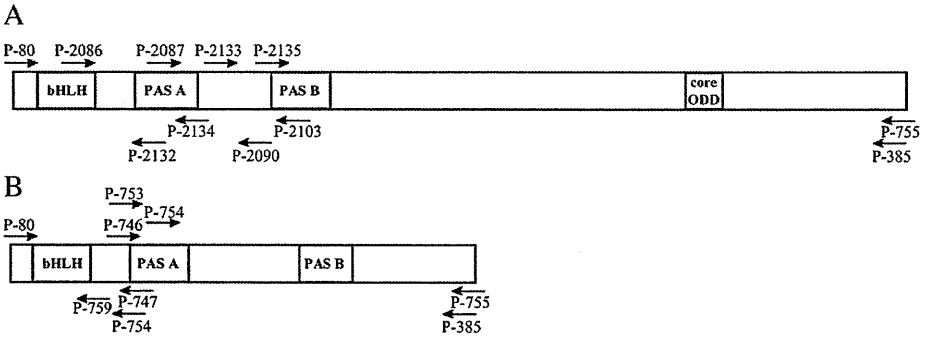

Fig. 2. Positions of primers designed for RT-PCR of (A) *A. suum* HIF-1α and (B) *A. suum* HIF-1β.

DNase I (Invitrogen) and quantified using the RiboGreen reagent (Molecular Probes) with a spectrofluorometer (Jasco FP-6300). Equal amounts (1 μg) of total RNAs were used as templates for reverse transcription with a SuperScript VILO synthesis kit (Invitrogen). Real-time PCR was carried out on a LightCycler (Roche) using QuantiTect SYBR Green PCR Master Mix (Qiagen). The PCR reaction was performed with 30 cycles of 94 °C for 15 s, 55 °C for 30 s, 72 °C for 10 s. Primers P-2582 and P-2134 were used for *hif-1α*, and P-753 and P-754 were used for *hif-1β*. Nucleotide sequences of the primers are shown in Table 1.

2.6. Normoxic and hypoxic exposure of A. suum worms

L3 and adult worms were incubated under either normoxic or hypoxic conditions for 16 hr at 37 °C. For hypoxic exposure, L3 and adult worms were soaked in phosphate buffered saline (PBS) and placed into the GasPak System (BBL). Parallel to hypoxic exposure, worms were soaked in PBS and placed into an incubator in the presence of air. According to the manufacturer's instruction for GasPak System, oxygen concentration decreases to less than 0.1% within 90 min, and the establishment of this condition was confirmed using a methylene blue indicator purchased from BBL. Total RNAs were extracted from triplicate samples of adult muscle and a single sample of L3.

2.7. Sequence analysis of 5′-upstream regions of complex II genes

Approximately 2 kb 5′-upstream sequences of the coding start sites of *A. suum* complex II subunit genes were analyzed. Genomic clones containing the corresponding regions were isolated from a lambda Fix II genomic library of *A. suum* by plaque hybridization using a digoxygenin (DIG)-labeled nucleotide probe. Each fragment was inserted into the pZErO-2 plasmid (Invitrogen) and sequenced (Operon).

3. Results

3.1. Cloning of A. suum hif-1α and hif-1β cDNAs

To obtain partial sequences of *A. suum hif-1α* and *hif-1β* cDNAs by RT-PCR, degenerate primers were designed based on conserved amino acid sequences corresponding to the bHLH and the PAS domains of vertebrate and invertebrate HIF-1s. Partial sequences of *A. suum hif-1α* cDNA were not amplified using these primers, while those of *hif-1β* were obtained. Then, the nematode EST database was searched for *hif-1α* homologs using amino acid sequences of *C. elegans* HIF-1 as a query, and degenerate primers were redesigned based on the conserved regions among nematode species: *C. elegans*, *S. ratti*, and *B. malayi*. As a result, partial sequences of *A. suum hif-1α* cDNA were amplified. Finally, by performing 5′RACE using the nematode spliced leader sequence SL1, and 3′RACE, the full-length *A. suum hif-1α* and *hif-1β* cDNAs were obtained.

The full-length *A. suum hif-1α* cDNA consists of 2861 bp, which contains 234 bp of 5′UTR, 2499 bp of open reading frame encoding 832 deduced amino acid residues, and 128 bp of 3′UTR including a polyA signal sequence (GenBank ID: AB520828). An alignment of the conserved N-terminal amino acid sequences of *A. suum* HIF-1α with those of *B. malayi*, *C. elegans*, *Daphnia magna*, *X. laevis*, and *H. sapiens* is shown in Fig. 3A. *A. suum* HIF-1α exhibits high sequence conservation in the bHLH, PAS-A, and PAS-B domains, which have 76%, 67%, and 59% identities to those of *C. elegans* HIF-1, respectively. In the C-terminal side of the PAS B domain, the core sequence of the ODD, which is essential for prolyl hydroxylation and generally contains an LXXLAP motif (X indicates any amino acid and P indicates the hydroxylacceptor proline) (Huang et al., 2002), was found (Fig. 3B). However, homologous sequences corresponding to neither the N-TAD nor the C-TAD were identified (Fig. 3C).

The full-length *A. suum hif-1β* cDNA consists of 1558 bp, which contains 50 bp of 5′UTR, 1308 bp of open reading frame encoding a deduced 435 amino acid residues, and 200 bp of 3′UTR including a polyA signal sequence (GenBank ID: AB520829). An alignment of the amino acid sequences of the full-length *A. suum* HIF-1β with those of other organisms is shown in Fig. 4A. The bHLH, PAS-A, and PAS-B domains are highly conserved in *A. suum* HIF-1β and show 96%, 70%, and 47% identities to those of *C. elegans* AHA-1 (*C. elegans* HIF-1β), respectively. On the other hand, the C-terminus of *A. suum* HIF-1β is significantly shorter than those of other organisms, and the CAD was not found (Fig. 4B).

3.2. Interaction between A. suum HIF-1α and HIF-1β

As described in previous reports on *H. sapiens* and *C. elegans* HIF-1s, canonical HIF-1 consists of HIF-1α and HIF-1β subunits, and their dimerization is essential for their binding to HREs (Jiang et al., 2001a; Kallio et al., 1997). To determine whether *A. suum* HIF-1 forms a similar complex, the interaction between *A. suum* HIF-1α and HIF-1β was analyzed by yeast two-hybrid assays. Yeast strain AH109 co-transformed with both plasmids pGADT7-GAL4-HIF-1α and pGBKT7-GAL4-HIF-1β grew on selective medium lacking adenine, histidine, leucine, and tryptophan, while cells expressing either pGADT7-GAL4-HIF-1α or pGBKT7-GAL4-HIF-1β formed no colonies (Fig. 5). The specific interaction between *A. suum* HIF-1α and HIF-1β indicates that these two proteins are binding partners.

3.3. Stage-specific expression of hif-1α and hif-1β mRNAs

A. suum fertilized eggs develop to L3 worms under normoxic conditions (150–160 mm Hg), while adult worms inhabit a hypoxic environment (0–10 mm Hg) (Kita and Takamiya, 2002; Takamiya et al., 1993). In order to determine if there is a regulatory relationship between *hif-1* expression and the oxygen conditions in different habitats, transcript levels of *hif-1α* and *hif-1β* were examined in the aerobic free-living stages and the anaerobic parasite stages by real-time PCR. As shown in Fig. 6, both *hif-1* mRNAs were expressed at all stages and most abundantly in aerobic free-living L3. *hif-1α* and *hif-1β* mRNA levels in L3 were 8-fold and 6-fold higher than those in adult muscle, respectively. In the parasite stages, both *hif-1* mRNAs gradually decreased as worms developed. In fertilized eggs, *hif-1α* mRNA expression was 6-fold higher than that of adult muscle, while *hif-1β* mRNA expression was slightly higher (1.2-fold) than that of adult muscle.

In hypoxia-tolerant organisms such as the mole rat *Spalax*, HIF-1α expression is induced by hypoxic exposure not only at the post-transcriptional but also at the transcriptional level (Rahman and Thomas, 2007; Shams et al., 2004). Although there is a report that the perienteric fluid of the adult worm was kept hypoxic even under normoxic conditions due to existence of oxygen-avid hemoglobin, it was suggested that at least some degree of oxygen diffused through muscle walls (Minning et al., 1999). In order to assess the effect of oxygen conditions on *hif-1* expression, transcript levels of *hif-1* mRNAs were compared between normoxia- and hypoxia-exposed L3 and adult worms (muscle tissue) by real-time PCR.16-hours incubation was adopted, because 12-hour and 16-hour exposures made no difference in expression of hypoxia-related genes in our preliminary study. Consequently, no significant difference was observed in either of the two groups as shown in Fig. 7.

3.4. Sequence analysis of 5′-upstream regions of A. suum complex II genes

The mammalian HIF-1 binds to specific DNA sequences called the HREs, which contain the sequence 5′-RCGTG (Wang and Semenza, 1993). Similarly, in *C. elegans*, a survey of the sequences 200–2000 bp 5′ upstream of the predicted translational start sites showed that the sequence 5′-TACGTG was present in 46% of *hif-1*-dependent genes (Shen et al., 2005).

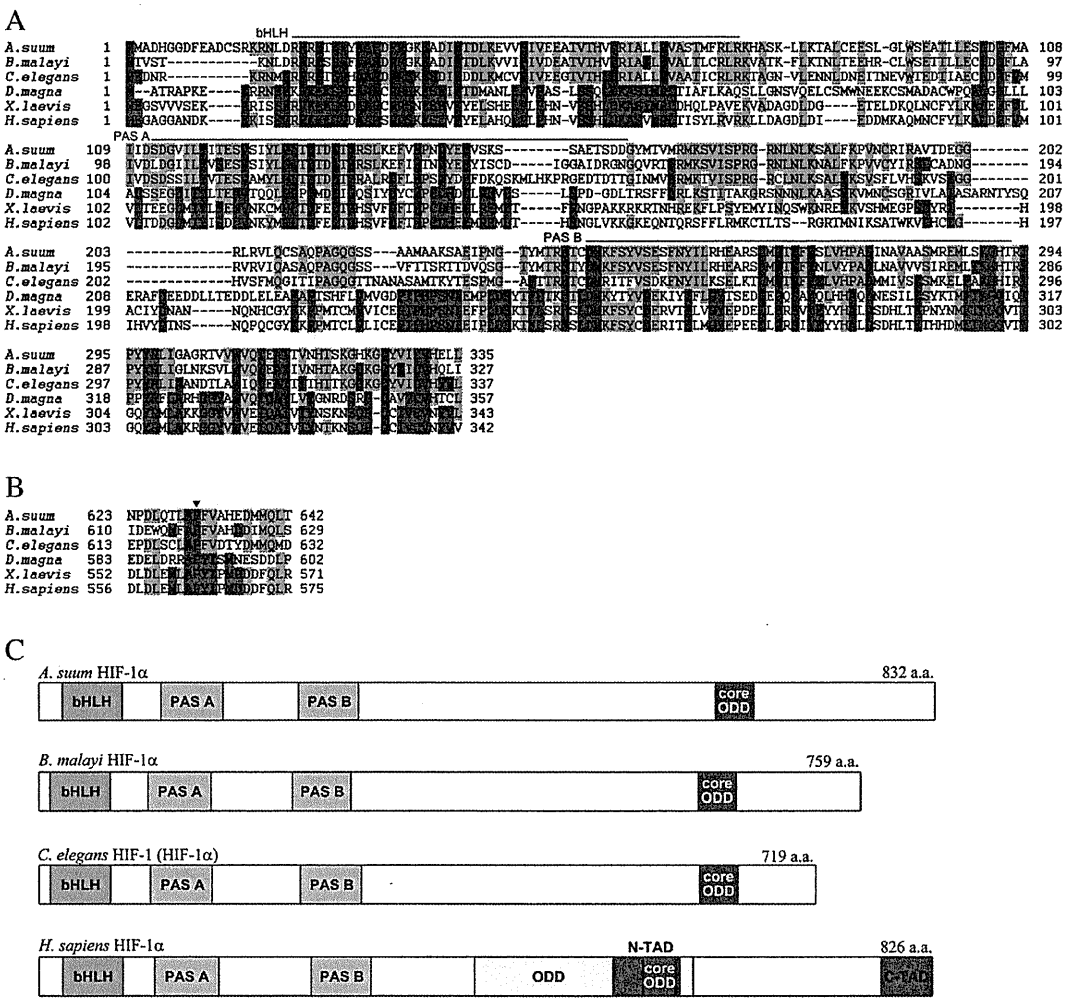

Fig. 3. Alignment of the deduced amino acid sequences of *A. suum* HIF-1α with homologs of other organisms. Amino acid sequences are designated by single-letter codes and numbered. Identical amino acid residues shared by all six species are highlighted in blue. Conserved residues in three species are shaded in green or pink whether including *A. suum* or not. Dashes indicate gaps introduced to facilitate alignment. (A) Conserved N-terminal amino acid sequences of HIF-1α. Black bars represent the bHLH, PAS-A, and PAS B domains. (B) Amino acid sequences around the core sequences of the ODD. The conserved proline residues are indicated by an arrowhead. (C) Domain structures of HIF-1α of nematodes (*A. suum*, *B. malayi*, and *C. elegans*) and humans.

Since the Fp and CybS subunits of *A. suum* complex II are expected to be target genes of HIF-1, nucleotide sequences of 5′-upstream regions of these genes were determined and searched for putative HREs on the assumption that the HRE motif is conserved between *C. elegans* and *A. suum*. Consequently, all the subunits except for adult-type Fp were found to possess putative HREs in their 5′-upstream regions (Fig. S1). Nucleotide sequences are available in the DDBJ/EMBL/GenBank databases under accession numbers AB626613–AB626618.

4. Discussion

Certain hypoxia-tolerant organisms are known to alter their metabolic pathways from aerobic-type to anaerobic-type in parallel with changes in the oxygen environment (Kita et al., 1997; Komuniecki and Harris, 1995; Tielens and Van Hellemond, 1998). *A. suum* is the biochemically best-characterized model organism among parasitic helminths and exhibits a prominent transition in carbohydrate metabolism during development. However, nothing is known about the regulatory mechanisms by which *A. suum* senses environmental oxygen concentrations and activates transcription of responsible genes for adaptation to hypoxia. The present study is the first report of cloning and characterization of *hif-1α* and *hif-1β* cDNAs from the parasitic helminth.

4.1. Cloning of *A. suum hif-1α* and *hif-1β* cDNAs

The predicted amino acid sequences of both *A. suum* HIF-1α and HIF-1β showed high levels of sequence conservation across phyla in the N-terminal regions from the bHLH domains to the PAS domains. During the preparation of this manuscript, the transcriptome information of *A. suum* was released (Wang et al., 2011), in which both HIF-1α and HIF-1β were annotated (GenBank ID: JI166617.1 and JI171286.1, respectively), and the deduced amino acid sequences of HIF-1α were exactly same as our result except for one amino acid at residue 754 (valine in our result and isoleucine in the transcriptome data). The core sequences of the ODD containing the LXXLAP motif are conserved in *A. suum* HIF-1α; in addition, homologous genes encoding PHD and VHL are found in the transcriptome analysis of *A. suum* (GenBank ID: JI165998.1 and JI165450.1, respectively) (Wang et al., 2011), supporting the hypothesis that *A. suum* HIF-1α is regulated by oxygen-dependent prolyl hydroxylation of the LXXLAP motif and functions as oxygen sensor as reported for *C. elegans* and humans (Epstein et al., 2001; Jaakkola et al., 2001). Our HIF-1β amino acid sequences were identical to the annotated HIF-1β from the transcriptome analysis between residues 1–433; however, they were 28 amino acids shorter in the N-terminus and 3 amino acids longer in the C-terminus. Because our HIF-1β sequences

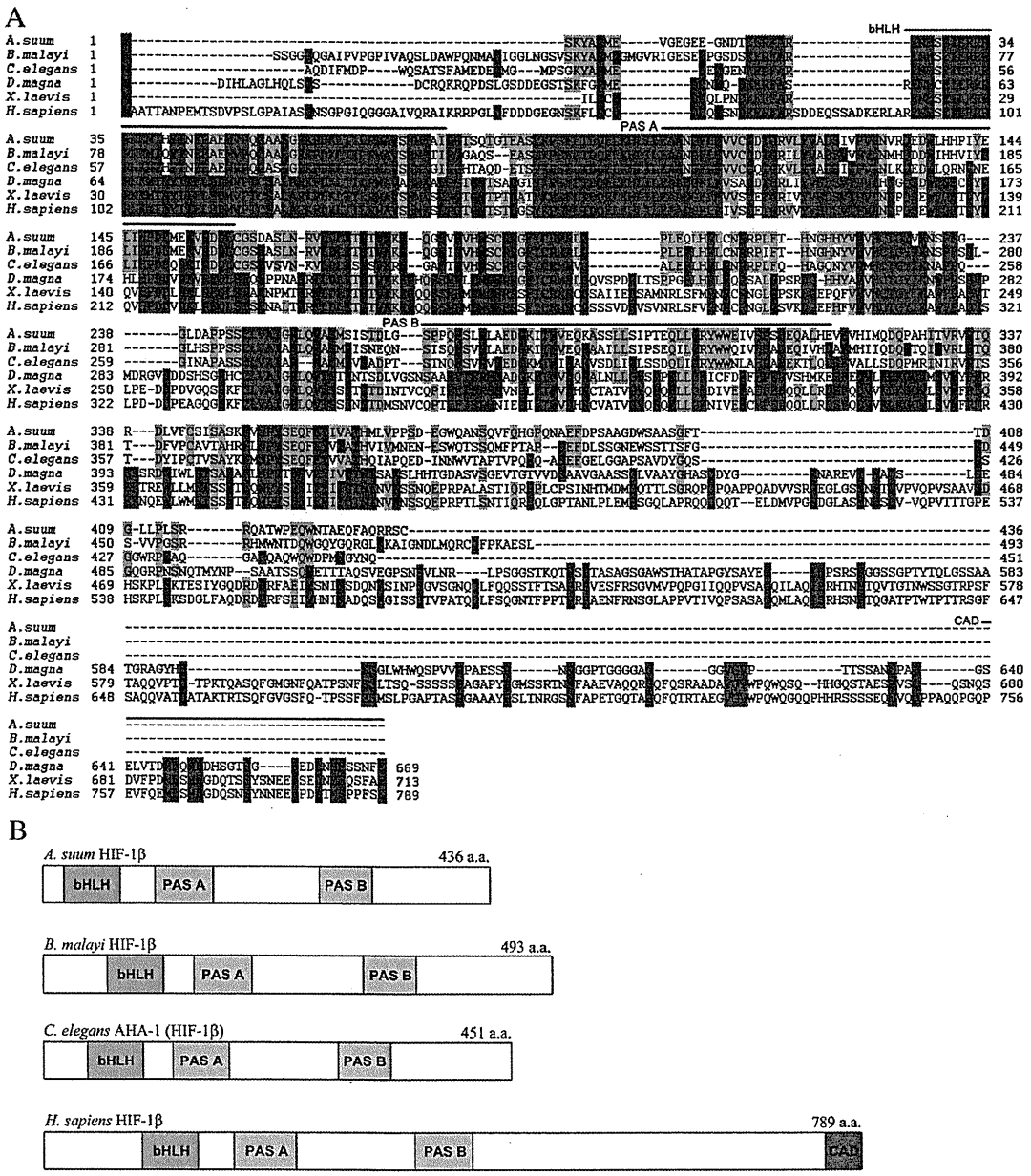

Fig. 4. (A) Alignment of the deduced amino acid sequences of *A. suum* HIF-1β with homologs of other organisms. Amino acid sequences are designated by single-letter codes and numbered. Identical amino acid residues shared by all six species are highlighted in blue. Conserved residues in three species are shaded in green or pink whether including *A. suum* or not. Dashes indicate gaps introduced to facilitate alignment. Black bars represent the bHLH, PAS-A, PAS B, and CAD domains. (B) Domain structures of HIF-1β of nematodes (*A. suum*, *B. malayi*, and *C. elegans*) and humans.

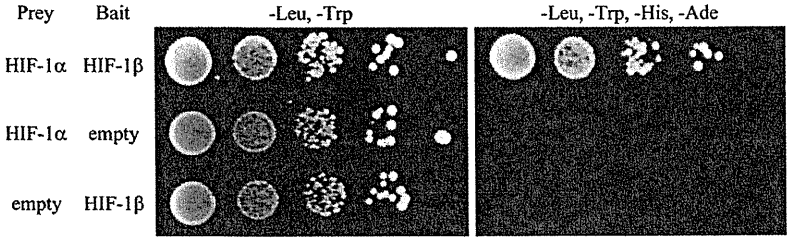

Fig. 5. Analysis of the interaction between *A. suum* HIF-1α and HIF-1β by yeast two-hybrid assays. Serial dilutions of yeast strains transformed with the indicated constructs were grown on plates lacking Leu and Trp as a control (left) and lacking Leu, Trp, His, and Ade (right).

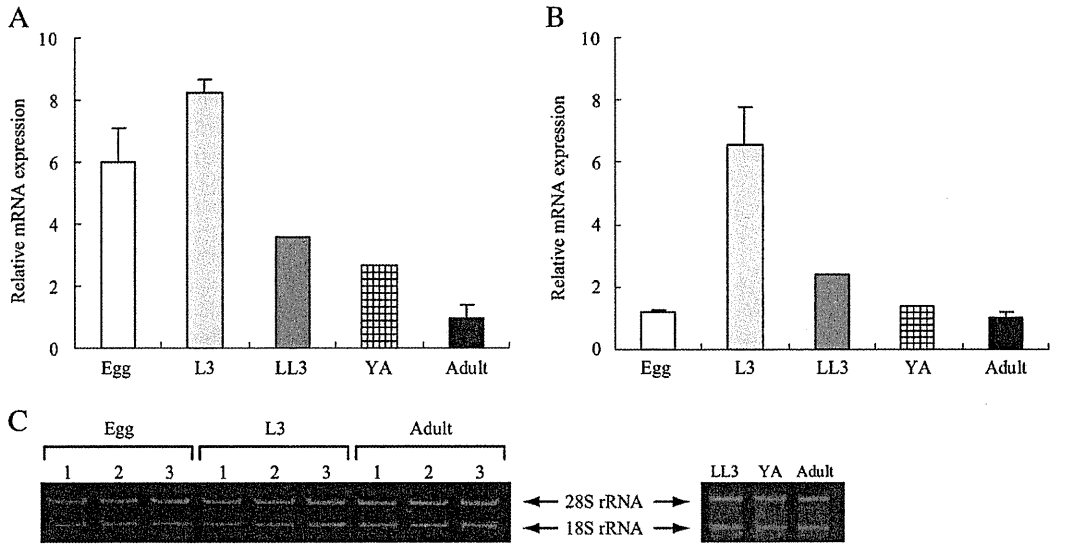

Fig. 6. Expression levels of *hif-1* mRNA at different developmental stages in *A. suum*. The ratios of mRNA levels in each sample to those in adult muscle are shown (A, *hif-1α* and B, *hif-1β* mRNA levels. C, 1 μg of total RNAs from each stage used for reverse transcription). Values are the means of three experiments ± SD. In fertilized eggs, the *hif-1α* level was 6-fold higher than that of adult muscle, while *hif-1β* showed only a slight difference between these two stages. *hif-1α* and *hif-1β* levels in L3 were 8-fold and 6-fold higher than those in adult muscle, respectively. In anaerobic parasite stages, both levels were gradually decreased during development.

contained both SL1 sequences and polyA signal sequences, it appears to exist as a processed transcript in adult worms, although there may be several splicing variants. In addition to the conservation of functionally important domains, the yeast two-hybrid assay indicated that *A. suum* HIF-1α and HIF-1β form a complex. These results strongly suggest that *A. suum* HIF-1α and HIF-1β dimerize and play an important role in adaptation to hypoxia.

In contrast to the sequence conservation in the N-terminal regions, *A. suum* HIF-1 subunits exhibited remarkable diversity in the C-terminal region of the PAS domains, except for the core sequences of the ODD in HIF-1α. *A. suum* HIF-1β is approximately 250 amino acids shorter than vertebrate HIF-1βs at the C-termini, and lacks the CAD. This property is commonly observed in other nematodes such as *B. malayi* and *C. elegans*. Because the CAD is conserved not only in vertebrates but also in arthropods, such as *D. melanogaster* and *D. magna* (Sonnenfeld et al., 1997; Tokishita et al., 2006), the CAD could have been evolutionarily lost from a common ancestor of nematode species. However, substantial induction of hypoxia-responsive genes occurs in *C. elegans* lacking the CAD (Epstein et al., 2001). Similarly, in mammals, the CAD is dispensable for transcriptional activation of both hypoxia-responsive and dioxin-responsive genes (Beischlag et al., 2004; Li et al., 1996). From these observations, *A. suum* HIF-1β lacking the CAD is suggested to be capable of inducing HIF-1 target genes.

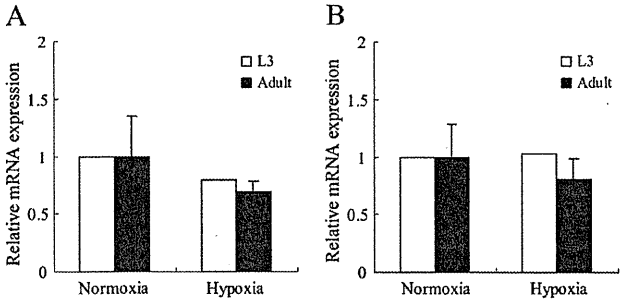

Fig. 7. Effects of hypoxic exposure on *hif-1α* and *hif-1β* mRNA levels in L3 and adult worms (muscle tissue). The ratios of mRNA levels in hypoxia-exposed worms to those in normoxia-exposed worms are shown (A, *hif-1α* and B, *hif-1β* mRNA levels). Values in adult worms are the means of three experiments ± SD.

Neither the N-TAD nor the C-TAD is identified in the C-terminal region of nematode HIF-1αs, and nematodes lack homologs of FIH-1, which in mammals catalyzes hydroxylation of a conserved asparagine residue in the C-TAD and represses HIF-1 transactivation in normoxia. This observation is consistent with a previous report claiming that no species have been identified wherein the C-TAD or FIH-1 is retained without the other (Hampton-Smith and Peet, 2009). Because the more phylogenetically basal *Acropora millepora* (*Cnidaria*) possesses functional FIH-1/C-TAD signaling (Hampton-Smith and Peet, 2009), nematodes appear to have lost the FIH-1 gene and the C-TAD from a common ancestor of nematode species, although their biological significance remains to be elucidated. Even compared with *B. malayi* and *C. elegans* HIF-1αs, the C-terminal region of *A. suum* HIF-1α is distinct in its length and shows no sequence similarity. In mammals, unlike the CAD, both the N-TAD and the C-TAD are essential for the recruitment of coactivators CBP/p300, SRC-1, and transcription intermediary factor 2 (TIF-2) (Gu et al., 2001; Lando et al., 2002a). While the C-TAD contributes to the regulation of most HIF target genes and is the predominant transactivation domain, the N-TAD confers HIF target gene specificity (Hu et al., 2007). The unique features of the C-terminal region of *A. suum* HIF-1α may shed light on new mechanisms of activation of HIF-1 and the regulation of target gene specificity.

4.2. Stage-specific expression of *hif-1α* and *hif-1β* mRNAs

Previous reports on *in vivo* expression patterns and the regulation of *hif-1α* and *hif-1β* mRNAs are controversial. It has been generally considered that both *hif-1* mRNAs are constitutively expressed and that the stability of HIF-1 is regulated primarily at the post-transcriptional level in an oxygen-dependent manner (Powell et al., 2002; Wang et al., 1995). However, conflicting reports have demonstrated that *hif-1α* and/or *hif-1β* mRNA expression are affected by oxygen concentrations in various organisms: rats, birds, and fish (Catron et al., 2001; Rahman and Thomas, 2007; Wiener et al., 1996). In these organisms, particularly in hypoxia-tolerant rats and fish, HIF-1α expression is upregulated at both the transcriptional and post-transcriptional level by hypoxic exposure (Rahman and Thomas, 2007; Shams et al., 2004).

A. suum is a unique model organism for investigating the relationship between *hif-1* expression and the oxygen conditions, since *A. suum* is exposed to normoxia and hypoxia in its natural habitat during its life cycle. To examine *in vivo* expression patterns of *A. suum hif-1α* and *hif-1β*, mRNA levels at different developmental stages were analyzed by real-time PCR. Fertilized eggs showed 6-fold higher *hif-1α* mRNA levels than adult muscle, while *hif-1β* mRNA expression was similar between eggs and adult muscle. This difference in expression patterns of *hif-1α* and *hif-1β* mRNAs could be attributed to their different roles in embryonic development.

In the free-living nematode *C. elegans*, microarray analysis of developmental gene expression have revealed that expression levels of *hif-1* and *aha-1* (*C. elegans hif-1β*) mRNAs are highest during the larval stage, but both show only 2-fold differences at maximum throughout the life cycle (Jiang et al., 2001b). In contrast, in *A. suum*, both *hif-1α* and *hif-1β* mRNA expression significantly changed during the life cycle. They reached maximum levels at the free-living L3 stage and were 6-fold and 8-fold higher than those during the adult stage, respectively. After infection of the host, both *hif-1* mRNAs gradually decreased with development. Significant transcriptional changes of *A. suum hif-1* indicate that there is a regulatory mechanism for its expression. Given that hypoxic exposure had no effects on *hif-1* mRNA levels at any investigated stages, transcriptions of *A. suum hif-1* appear to be regulated in a stage-specific manner rather than in an oxygen-dependent manner. In the hypoxia-tolerant mole rat *Spalax*, *hif-1α* transcription is induced by hypoxia; however, even in normoxia, *Spalax* maintains 2-fold higher *hif-1α* mRNA levels than that in the hypoxia-sensitive rat *Rattus*, enabling effective responses to hypoxia (Shams et al., 2004). These findings imply that certain hypoxia-tolerant organisms accumulate *hif-1* mRNAs even under normoxia. In *A. suum*, high levels of *hif-1* mRNAs in L3 possibly allow quick and sufficient responses to a sudden change of oxygen concentration after ingestion by the host by regulating genes responsible for anaerobic energy metabolism.

4.3. Hypoxia-responsive elements located in 5′-upstream regions of A. suum complex II genes

One of the characteristic features of the HIF-1 pathway is its broad range of target genes. One subset of target genes regulated by HIF-1 encodes various glycolytic enzymes that are robustly upregulated during hypoxia, contributing to metabolic adaptation (Bunn and Poyton, 1996; Seagroves et al., 2001). In addition, recent studies have demonstrated functional crosstalk between the HIF pathway and mitochondria.

In human cells, HIF-1 regulates the replacement of a key subunit of the mitochondrial cytochrome *c* oxidase (COX, also known as complex IV) from COX4-1 to COX4-2 to maximize the efficiency of mitochondrial respiration under hypoxia (Fukuda et al., 2007). Conversely, it has been shown that inhibition of SDH activity (activity of aerobic complex II) results in the accumulation of succinate in the cells, which reduces the enzymatic activity of prolyl hydroxylases by product inhibition. This leads to HIF-1α stabilization and consequently HIF-1 activation (Selak et al., 2005).

Our previous study showed that the expression of the stage-specific isoforms of *A. suum* complex II is regulated at the transcriptional level, enabling metabolic adaptation to hypoxia in the host (Amino et al., 2000, 2003). Considering the importance of structural rearrangements of complex II under hypoxic conditions, a regulatory mechanism between HIF-1 and the expression of complex II subunits is expected to be present. Sequence analysis of 5′-upstream regions of complex II genes identified putative HREs, suggesting that HIF-1 directly regulates the expression of stage-specific complex II isoforms, although the expression of the adult-type Fp appears to be regulated by other factors regardless of hypoxia.

5. Conclusions

In the present study, we cloned *hif-1* cDNAs from *A. suum* and found unique characteristics of their expression patterns. Stage-specific *hif-1* expression may reflect an evolved strategy for hypoxia adaptation, although the regulatory mechanisms are yet to be elucidated. The N-TAD of HIF-1α showed unique sequences distinct from those of other organisms, suggesting that target genes of *A. suum* HIF-1 may be different from known targets. Although further investigation is required to determine the functional role of *A. suum* HIF-1 in the adaptation to hypoxic conditions of adult worms, we consider that it is plausible that HIF-1 is associated with stage-specific metabolic transitions, including the rearrangement of the complex II structure.

Adaptation to changes in the oxygen environment is an important aspect of parasitism, and studies of its regulatory mechanisms will reveal adaptive strategies of parasites in the host.

Supplementary data to this article can be found online at http://dx.doi.org/10.1016/j.gene.2012.12.025.

Acknowledgments

We thank Dr. Takeshi Hatta and Dr. Takeharu Miyoshi for technical support with animal experiments. This study was mainly supported by in part by a Grant-in-aid for Creative Scientific Research (Grant 18GS0314), a Grant-in-aid for Scientific Research on Priority Areas (18073004) from the Japanese Society for the Promotion of Science, the Targeted Proteins Research Program from the Japanese Ministry of Education, Science, Culture, Sports and Technology (MEXT), for research on emerging and re-emerging infectious diseases from the Japanese Ministry of Health and Welfare, and partly by the Programme for Promotion of Basic and Applied Researches for Innovations in Bio-oriented Industry (BRAIN).

References

Amino, H., et al., 2000. Stage-specific isoforms of *Ascaris suum* complex II: the fumarate reductase of the parasitic adult and the succinate dehydrogenase of free-living larvae share a common iron-sulfur subunit. Mol. Biochem. Parasitol. 106, 63–76.

Amino, H., et al., 2003. Isolation and characterization of the stage-specific cytochrome b small subunit (CybS) of *Ascaris suum* complex II from the aerobic respiratory chain of larval mitochondria. Mol. Biochem. Parasitol. 128, 175–186.

Beischlag, T., et al., 2004. Recruitment of thyroid hormone receptor/retinoblastoma-interacting protein 230 by the aryl hydrocarbon receptor nuclear translocator is required for the transcriptional response to both dioxin and hypoxia. J. Biol. Chem. 279, 54620–54628.

Bunn, H., Poyton, R., 1996. Oxygen sensing and molecular adaptation to hypoxia. Physiol. Rev. 76, 839–885.

Catron, T., Mendiola, M., Smith, S., Born, J., Walker, M., 2001. Hypoxia regulates avian cardiac Arnt and HIF-1alpha mRNA expression. Biochem. Biophys. Res. Commun. 282, 602–607.

Chomczynski, P., Sacchi, N., 1987. Single-step method of RNA isolation by acid guanidinium thiocyanate-phenol-chloroform extraction. Anal. Biochem. 162, 156–159.

Epstein, A., et al., 2001. *C. elegans* EGL-9 and mammalian homologs define a family of dioxygenases that regulate HIF by prolyl hydroxylation. Cell 107, 43–54.

Fukuda, R., Zhang, H., Kim, J., Shimoda, L., Dang, C., Semenza, G., 2007. HIF-1 regulates cytochrome oxidase subunits to optimize efficiency of respiration in hypoxic cells. Cell 129, 111–122.

Gu, J., Milligan, J., Huang, L., 2001. Molecular mechanism of hypoxia-inducible factor 1alpha -p300 interaction. A leucine-rich interface regulated by a single cysteine. J. Biol. Chem. 276, 3550–3554.

Hampton-Smith, R., Peet, D., 2009. From polyps to people: a highly familiar response to hypoxia. Ann. N. Y. Acad. Sci. 1177, 19–29.

Hu, C.J., Sataur, A., Wang, L., Chen, H., Simon, M.C., 2007. The N-terminal transactivation domain confers target gene specificity of hypoxia-inducible factors HIF-1alpha and HIF-2alpha. Mol. Biol. Cell 18, 4528–4542.

Huang, J., Zhao, Q., Mooney, S., Lee, F., 2002. Sequence determinants in hypoxia-inducible factor-1alpha for hydroxylation by the prolyl hydroxylases PHD1, PHD2, and PHD3. J. Biol. Chem. 277, 39792–39800.

Islam, M.K., et al., 2006. Effect of piperazine (diethylenediamine) on the moulying proteome express and pyrophosphate activity of *Ascaris suum* lung-stage larvae. Acta Trop. 99, 208–217.

Ivan, M., et al., 2001. HIFalpha targeted for VHL-mediated destruction by proline hydroxylation: implications for O_2 sensing. Science 292, 464–468.

Iwata, F., et al., 2008. Change of subunit composition of mitochondrial complex II (succinate–ubiquinone reductase/quinol–fumarate reductase) in *Ascaris suum* during the migration in the experimental host. Parasitol. Int. 57, 54–61.
Jaakkola, P., et al., 2001. Targeting of HIF-alpha to the von Hippel–Lindau ubiquitylation complex by O_2-regulated prolyl hydroxylation. Science 292, 468–472.
Jain, S., Dolwick, K., Schmidt, J., Bradfield, C., 1994. Potent transactivation domains of the Ah receptor and the Ah receptor nuclear translocator map to their carboxyl termini. J. Biol. Chem. 269, 31518–31524.
Jiang, B., Rue, E., Wang, G., Roe, R., Semenza, G., 1996. Dimerization, DNA binding, and transactivation properties of hypoxia-inducible factor 1. J. Biol. Chem. 271, 17771–17778.
Jiang, B., Zheng, J., Leung, S., Roe, R., Semenza, G., 1997. Transactivation and inhibitory domains of hypoxia-inducible factor 1alpha. Modulation of transcriptional activity by oxygen tension. J. Biol. Chem. 272, 19253–19260.
Jiang, H., Guo, R., Powell-Coffman, J., 2001a. The *Caenorhabditis elegans hif-1* gene encodes a bHLH-PAS protein that is required for adaptation to hypoxia. Proc. Natl. Acad. Sci. U. S. A. 98, 7916–7921.
Jiang, M., Ryu, J., Kiraly, M., Duke, K., Reinke, V., Kim, S., 2001b. Genome-wide analysis of developmental and sex-regulated gene expression profiles in *Caenorhabditis elegans*. Proc. Natl. Acad. Sci. U. S. A. 98, 218–223.
Kaelin, W.J., Ratcliffe, P., 2008. Oxygen sensing by metazoans: the central role of the HIF hydroxylase pathway. Mol. Cell 30, 393–402.
Kallio, P., Pongratz, I., Gradin, K., McGuire, J., Poellinger, L., 1997. Activation of hypoxia-inducible factor 1alpha: posttranscriptional regulation and conformational change by recruitment of the Arnt transcription factor. Proc. Natl. Acad. Sci. U. S. A. 94, 5667–5672.
Kallio, P., et al., 1998. Signal transduction in hypoxic cells: inducible nuclear translocation and recruitment of the CBP/p300 coactivator by the hypoxia-inducible factor-1alpha. EMBO J. 17, 6573–6586.
Kita, K., Takamiya, S., 2002. Electron-transfer complexes in *Ascaris* mitochondria. Adv. Parasitol. 51, 95–131.
Kita, K., Hirawake, H., Takamiya, S., 1997. Cytochromes in the respiratory chain of helminth mitochondria. Int. J. Parasitol. 27, 617–630.
Kita, K., Hirawake, H., Miyadera, H., Amino, H., Takeo, S., 2002. Role of complex II in anaerobic respiration of the parasite mitochondria from *Ascaris suum* and *Plasmodium falciparum*. Biochim. Biophys. Acta 1553, 123–139.
Komuniecki, R., Harris, B.G., 1995. Carbohydrate and energy metabolism in helminths. In: Marr, J., Mueller, M. (Eds.), Biochemistry and Molecular Biology of Parasites. Academic Press, London, pp. 49–66.
Lando, D., Peet, D., Whelan, D., Gorman, J., Whitelaw, M., 2002a. Asparagine hydroxylation of the HIF transactivation domain a hypoxic switch. Science 295, 858–861.
Lando, D., Peet, D., Gorman, J., Whelan, D., Whitelaw, M., Bruick, R., 2002b. FIH-1 is an asparaginyl hydroxylase enzyme that regulates the transcriptional activity of hypoxia-inducible factor. Genes Dev. 16, 1466–1471.
Li, H., Ko, H., Whitlock, J., 1996. Induction of phosphoglycerate kinase 1 gene expression by hypoxia. Roles of Arnt and HIF1alpha. J. Biol. Chem. 271, 21262–21267.
Minning, D.M., et al., 1999. *Ascaris* haemoglobin is a nitric oxide-activated 'deoxygenase'. Nature 401, 497–502.
Nilsen, T., et al., 1989. Characterization and expression of a spliced leader RNA in the parasitic nematode *Ascaris lumbricoides* var. *suum*. Mol. Cell. Biol. 9, 3543–3547.
Powell, J., Elshtein, R., Forest, D., Palladino, M., 2002. Stimulation of hypoxia-inducible factor-1 alpha (HIF-1alpha) protein in the adult rat testis following ischemic injury occurs without an increase in HIF-1alpha messenger RNA expression. Biol. Reprod. 67, 995–1002.
Powell-Coffman, J., Bradfield, C., Wood, W., 1998. *Caenorhabditis elegans* orthologs of the aryl hydrocarbon receptor and its heterodimerization partner the aryl hydrocarbon receptor nuclear translocator. Proc. Natl. Acad. Sci. U. S. A. 95, 2844–2849.
Pugh, C., O'Rourke, J., Nagao, M., Gleadle, J., Ratcliffe, P., 1997. Activation of hypoxia-inducible factor-1; definition of regulatory domains within the alpha subunit. J. Biol. Chem. 272, 11205–11214.
Rahman, M., Thomas, P., 2007. Molecular cloning, characterization and expression of two hypoxia-inducible factor alpha subunits, HIF-1alpha and HIF-2alpha, in a hypoxia-tolerant marine teleost, Atlantic croaker (*Micropogonias undulatus*). Gene 396, 273–282.
Sakai, C., Tomitsuka, E., Esumi, H., Harada, S., Kita, K., 2012. Mitochondrial fumarate reductase as a target of chemotherapy: from parasites to cancer cells. Biochim. Biophys. Acta 1820, 643–651.
Saruta, F., et al., 1995. Stage-specific isoforms of complex II (succinate–ubiquinone oxidoreductase) in mitochondria from the parasitic nematode, Ascaris suum. J. Biol. Chem. 270, 928–932.
Seagroves, T.N., et al., 2001. Transcription factor HIF-1 is a necessary mediator of the Pasteur effect in mammalian cells. Mol. Cell. Biol. 21, 3436–3444.
Selak, M.A., et al., 2005. Succinate links TCA cycle dysfunction to oncogenesis by inhibiting HIF-alpha prolyl hydroxylase. Cancer Cell 7, 77–85.
Semenza, G., 2011. Oxygen sensing, homeostasis, and disease. N. Engl. J. Med. 365, 537–547.
Shams, I., Avivi, A., Nevo, E., 2004. Hypoxic stress tolerance of the blind subterranean mole rat: expression of erythropoietin and hypoxia-inducible factor 1 alpha. Proc. Natl. Acad. Sci. U. S. A. 101, 9698–9703.
Shen, C., Nettleton, D., Jiang, M., Kim, S., Powell-Coffman, J., 2005. Roles of the HIF-1 hypoxia-inducible factor during hypoxia response in *Caenorhabditis elegans*. J. Biol. Chem. 280, 20580–20588.
Shimizu, H., et al., 2012. Crystal structure of mitochondrial quinol-fumarate reductase from the parasitic nematode *Ascaris suum*. J. Biochem. 151, 589–592.
Sonnenfeld, M., Ward, M., Nystrom, G., Mosher, J., Stahl, S., Crews, S., 1997. The *Drosophila* tango gene encodes a bHLH-PAS protein that is orthologous to mammalian Arnt and controls CNS midline and tracheal development. Development 124, 4571–4582.
Takamiya, S., et al., 1993. Developmental changes in the respiratory chain of *Ascaris* mitochondria. Biochim. Biophys. Acta 1141, 65–74.
Tielens, A., Van Hellemond, J., 1998. The electron transport chain in anaerobically functioning eukaryotes. Biochim. Biophys. Acta 1365, 71–78.
Tokishita, S., et al., 2006. Tissue-specific expression of a bHLH-PAS protein homologous to ARNT during the development of crustacean *Daphnia magna*. Gene 376, 231–239.
Wang, G., Semenza, G., 1993. Characterization of hypoxia-inducible factor 1 and regulation of DNA binding activity by hypoxia. J. Biol. Chem. 268, 21513–21518.
Wang, G., Jiang, B., Rue, E., Semenza, G., 1995. Hypoxia-inducible factor 1 is a basic-helix-loop-helix-PAS heterodimer regulated by cellular O_2 tension. Proc. Natl. Acad. Sci. U. S. A. 92, 5510–5514.
Wang, J., et al., 2011. Deep small RNA sequencing from the nematode *Ascaris* reveals conservation, functional diversification, and novel developmental profiles. Genome Res. 21, 1462–1477.
Wiener, C., Booth, G., Semenza, G., 1996. *In vivo* expression of mRNAs encoding hypoxia-inducible factor 1. Biochem. Biophys. Res. Commun. 225, 485–488.
Zelzer, E., Wappner, P., Shilo, B., 1997. The PAS domain confers target gene specificity of *Drosophila* bHLH/PAS proteins. Genes Dev. 11, 2079–2089.

Biochimica et Biophysica Acta xxx (2013) xxx–xxx

Contents lists available at SciVerse ScienceDirect

Biochimica et Biophysica Acta

journal homepage: www.elsevier.com/locate/bbabio

Review

Diversity of parasite complex II☆

Shigeharu Harada [a,*], Daniel Ken Inaoka [b], Junko Ohmori [b], Kiyoshi Kita [b,**]

[a] Department of Applied Biology, Graduate School of Science and Technology, Kyoto Institute of Technology, Kyoto 606-8585, Japan
[b] Department of Biomedical Chemistry, Graduate School of Medicine, The University of Tokyo, Tokyo 113-0033, Japan

ARTICLE INFO

Article history:
Received 16 October 2012
Received in revised form 7 January 2013
Accepted 9 January 2013
Available online xxxx

Keywords:
Complex II
Fumarate respiration
Ascaris suum
Trypanosoma cruzi
Chemotherapy
Drug design

ABSTRACT

Parasites have developed a variety of physiological functions necessary for completing at least part of their life cycles in the specialized environments of surrounding the parasites in the host. Regarding energy metabolism, which is essential for survival, parasites adapt to the low oxygen environment in mammalian hosts by using metabolic systems that are very different from those of the hosts. In many cases, the parasite employs aerobic metabolism during the free-living stage outside the host but undergoes major changes in developmental control and environmental adaptation to switch to anaerobic energy metabolism. Parasite mitochondria play diverse roles in their energy metabolism, and in recent studies of the parasitic nematode, *Ascaris suum*, the mitochondrial complex II plays an important role in anaerobic energy metabolism of parasites inhabiting hosts by acting as a quinol-fumarate reductase. In Trypanosomes, parasite complex II has been found to have a novel function and structure. Complex II of *Trypanosoma cruzi* is an unusual supramolecular complex with a heterodimeric iron–sulfur subunit and seven additional non-catalytic subunits. The enzyme shows reduced binding affinities for both substrates and inhibitors. Interestingly, this structural organization is conserved in all trypanosomatids. Since the properties of complex II differ across a wide range of parasites, this complex is a potential target for the development of new chemotherapeutic agents. In this regard, structural information on the target enzyme is essential for the molecular design of drugs.
This article is part of a Special Issue entitled: Respiratory complex II: Role in cellular physiology and disease.

1. Introduction

1.1. Molecular parasitology

Parasites are classified generally as either helminths or protozoans. Helminths are multi-cellular parasites and are divided into three types: nematodes (e.g., *Ascaris suum*), trematodes (e.g., *Schistosoma japonica*), and cestodes (e.g., *Diphyllobothrium latum*). Protozoans include unicellular parasites (e.g., malaria parasites and *Entamoeba histolytica*), but they differ from bacteria in that they have a nucleus, mitochondria, vacuole, and other organelles (e.g., apicoplast, hydrogenosomes, and mitosomes). These parasites are capable of surviving and proliferating due to avoidance of host defense mechanisms and development of metabolic pathways adapted to the specialized environments of the host [see reviews 1–5].

Studies of parasitic adaptation have yielded extremely informative biological discoveries and data that are potentially useful for developing treatments of infectious diseases. Recent advances in biochemistry and molecular biology have provided new insights into basic parasite biology and have led to many revolutionary discoveries concerning biological evolution and diversity. Taken together, a new field called 'molecular parasitology' is being established to investigate parasitism at the molecular level. The unique features of parasite complex II have been revealed through data obtained through such a pioneering sciences [1,4,5].

1.2. Functional and subunit changes of complex II during the A. suum life cycle

The nematode *A. suum* has been studied extensively as a representative of human and livestock parasites [1]. During its life cycle, *A. suum* transitions from aerobic to anaerobic metabolism, reflecting the change in the environmental oxygen concentration (Fig. 1) [2–7]. During development from a fertilized egg to third stage larvae (L3) outside of the host, metabolism is aerobic as the tissues of mammalian host in that ATP is synthesized by aerobic oxidative phosphorylation [8]. In contrast,

Abbreviations: PEPCK, phosphoenolpyruvate carboxykinase; RQ, rhodoquinone; QFR, quinol-fumarate reductase; Fp, flavoprotein; FAD, flavin adenine dinucleotide; Ip, iron–sulfur protein; CybL, large subunit of cytochrome *b*; CybS, small subunit of cytochrome *b*; SDH, succinate dehydrogenase; UQ, ubiquinone; SQR, succinate-ubiquinone reductase; MK, menaquinone; RQH_2, rhodoquinol; FRD, fumarate reductase; OAA, oxaloacetate

☆ This article is part of a Special Issue entitled: Respiratory complex II: Role in cellular physiology and disease.

* Correspondence to: S. Harada, Department of Applied Biology, Graduate School of Science and Technology, Kyoto Institute of Technology, Sakyo-ku, Kyoto 606-8585, Japan. Tel.: +81 75 724 7541; fax: +81 75 724 7541.
** Correspondence to: K. Kita, Department of Biomedical Chemistry, Graduate School of Medicine, The University of Tokyo, Hongo, Bunkyo-ku, Tokyo 113-0033, Japan. Tel.: +81 3 5841 3526; fax: +81 3 5841 3444.
E-mail addresses: harada@kit.ac.jp (S. Harada), kitak@m.u-tokyo.ac.jp (K. Kita).

0005-2728/$ – see front matter © 2013 Published by Elsevier B.V.
http://dx.doi.org/10.1016/j.bbabio.2013.01.005

adult worms, which live in a low-oxygen environment, use the anaerobic phosphoenolpyruvate carboxykinase (PEPCK)-succinate pathway. The last step of the PEPCK-succinate pathway involves the NADH-fumarate reductase system, which is composed of complex I (NADH-quinone reductase), low-potential rhodoquinone (RQ), and complex II (quinol-fumarate reductase, QFR) [4,9]. Electron transfer from NADH to fumarate is coupled to ATP synthesis by site I phosphorylation in complex I. The difference in redox potential between NAD^+/NADH ($Em' = -320$ mV) and fumarate/succinate ($Em' = +30$ mV) is sufficient to drive ATP synthesis [4].

In eukaryotes, complex II is localized in the inner mitochondrial membrane and is generally composed of four peptides [4]. The largest flavoprotein (Fp, SDHA) subunit has a molecular mass of about 70 kDa and contains flavin adenine dinucleotide (FAD) as a prosthetic group. The relatively hydrophilic catalytic region of complex II is formed by the Fp subunit and the iron–sulfur cluster (Ip, SDHB) subunit, which has a molecular weight of about 30 kDa. The remaining subunits comprise cytochrome *b*, which contains heme *b*. Cytochrome *b* is composed of 2 hydrophobic membrane-anchoring polypeptide subunits: the 15 kDa large subunit (CybL, SDHC) and the 13 kDa small subunit (CybS, SDHD). These cytochrome *b* subunits are necessary for the interaction between complex II and hydrophobic membrane-associated quinones, such as ubiquinone (UQ) and RQ [6].

In a previous study, we showed that *A. suum* mitochondria express stage-specific isoforms of complex II [6,7,10]. While there are no differences in the isoforms of the Ip and CybL subunits of complex II between L3 larvae and adult *A. suum*, there are different isoforms of the complex II subunits Fp (larval, Fp^L; adult, Fp^A) and CybS (larval, $CybS^L$; adult, $CybS^A$) [7]. Quinone species in the mitochondria also differ during the life cycle of *A. suum*. In the adult mitochondria, the predominant quinone is the low-potential RQ ($Em' = -63$ mV); in larvae, the predominant quinone is UQ ($Em' = +110$ mV) [11]. Similarly, *Escherichia coli* and other bacteria show shifts in the combination of succinate-ubiquinone reductase (SQR) and UQ, and that of QFR and a low-potential quinone, such as menaquinone (MK) or RQ, during metabolic adaptation to changes in oxygen supply [12,13]. UQ has a higher redox potential than RQ; therefore, RQ is better suited to transferring electrons to fumarate than is UQ. In L2 and L3 *A. suum* larvae, UQ preferentially donates electrons to the cytochrome chain in the mitochondria. Thus, UQ participates in aerobic metabolism in *A. suum* larvae, whereas RQ participates in anaerobic metabolism in adult *A. suum* [11].

After being ingested by the definitive host, the L3 larvae penetrate the intestinal wall and reach the lung by migrating through other tissues, such as liver and heart. The L3 larvae pass from the lung via the trachea to the small intestine where they molt to L4 and develop into sexually maturate adult worms in the small intestine [14]. Protein chemical analysis reveals that the change in complex II begins with the anchor CybS subunit and then the Fp subunit [15].

1.3. Parasite complex II

Complex II molecules are classified into four types (Type A–D) and three classes (Class 1–3) according to the architecture of membrane anchors and functions *in vivo*, respectively [16]. The membrane anchor of Type A complex II consists of two polypeptide chains each having three transmembrane helices and two protoheme IX (heme *b*) molecules. Type B has one polypeptide chain with five transmembrane helices and two heme *b* molecules. On the other hand, Type C and D, like Type A, consist of two polypeptide chains with one and no heme *b* molecules in their anchors, respectively. In addition, more recent physiological analysis indicates novel Type E complex II [17], which is different from Type A–D in membrane-anchoring subunits and the composition of iron–sulfur centers. Class 1 complex II functions as SQR *in vivo* and catalyzes the oxidation of succinate and the reduction of high potential quinone, typically ubiquinone, whereas Class 2 complex II (QFR) catalyzes the opposite reaction, the oxidation of low potential quinol such as menaquinol and rhodoquinol (RQH_2) and the reduction of fumarate. Complex II belonging to Class 3, like the Class 1 enzymes, exhibits SQR activity but reduces low potential quinone. Crystal structures of complex II have been determined for three QFRs from *E. coli* (pdb code, 1L0V; [18]), *Wolinella succinogenes* (1QLB; [19]) and *A. suum* (3VR8; [20]), three SQRs from *E. coli* (1NEK; [21]), porcine (1ZOY; [22]) and chicken (1YQ3; [23]). QFRs from *E. coli*, *W. succinogenes*, and *A. suum* belong to Type D, Type B and Type C,

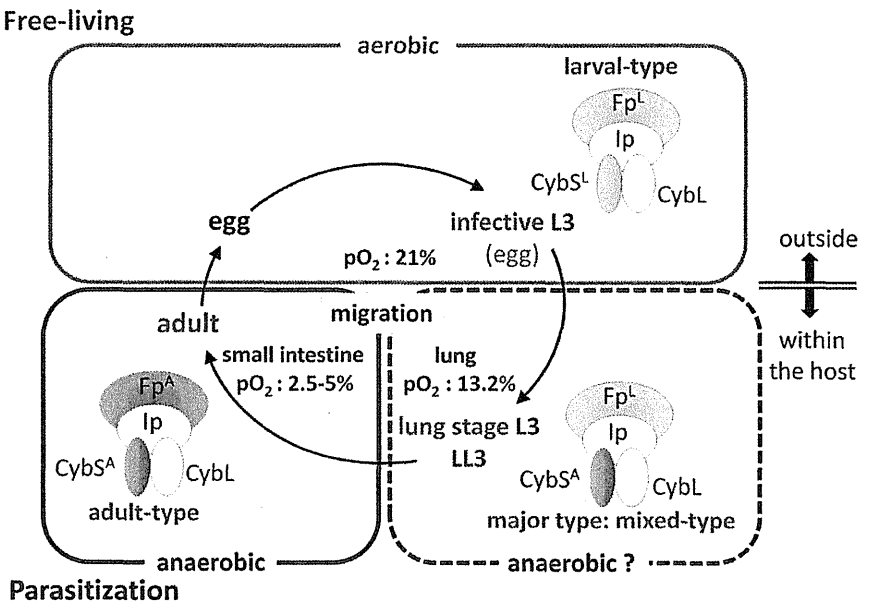

Fig. 1. Life cycle of *A. suum*. Fertilized eggs grow to infective L3 under an aerobic environment. Infective L3 larvae are ingested by the host, reach the small intestine and hatch there. Afterwards, larvae migrate into the host body (liver, heart, lung, and pharynx), and finally migrate back to the small intestine and develop into adults. In the host small intestine, the oxygen concentration is only 2.5% to 5% of that of the exogenous environment. During the life cycle, complex II molecules are expressed as stage-specific isoforms, larval-type, mixed-type and adult-type [15].

Please cite this article as: S. Harada, et al., Diversity of parasite complex II, Biochim. Biophys. Acta (2013), http://dx.doi.org/10.1016/j.bbabio.2013.01.005

respectively, whereas SQRs from porcine, chicken and *E. coli* are the Type C enzymes.

In general, the complex II molecules of helminthes, which are multi-cellular parasites, are of Type C, although catalytic function changes during the life cycle as mentioned above. However, complex II purified from the parasitic protist, *Trypanosoma cruzi*, consists of six hydrophilic and six hydrophobic nuclear-encoded subunits [24]. Notably, the iron–sulfur subunit is heterodimeric; $SDH2_N$ and $SDH2_C$ contain plant-type ferredoxin domains in the *N*-terminal half and bacterial ferredoxin domains in the C-terminal half, respectively.

In the case of malaria parasites, such as *Plasmodium falciparum*, anchor subunits of complex II have not yet been identified, although the enzyme shows SQR activity [25]. These unusual features of parasite complex II molecules make them targets for new chemotherapeutic agents.

In this review, we mainly focus on recent advances in the study of *A. suum* complex II, which plays an important role in the anaerobic energy metabolism of parasites. In addition, the molecular architecture of 12 novel complex II subunits of *T. cruzi* will be discussed.

2. Structure of adult *A. suum* QFR

Anaerobic mitochondrial complex II from adult *A. suum* (*A. suum* QFR) belongs to Type C/Class 2 and couples the oxidation of RQH_2 to RQ to the reduction of fumarate to succinate, an opposite reaction catalyzed by SQR of the aerobic respiratory chain [7]. We crystallized *A. suum* QFR in the presence of malonate [26], a well-known competitive inhibitor against complex II in various organisms and determined the crystal structure at 2.8 Å resolution (3VR8; [20]) by molecular replacement using the structure of porcine SQR (1ZOY; [22]) as the search model. In addition, the structure of the ternary complex with fumarate and flutolanil was determined at 2.9 Å resolution (3VRB; [20]). Flutolanil is a widely used commercially available fungicide [27] that specifically inhibits *A. suum* QFR as shown by IC_{50} values for *A. suum* QFR of 58 nM and porcine SQR of 46 μM. Based on these structures, as well as the structure of porcine SQR in complex with flutolanil (3AE8), the enzymatic mechanism of *A. suum* QFR and the structural basis of the specificity of flutolanil against *A. suum* QFR will be discussed.

2.1. Overall structure

The structure of *A. suum* QFR, the first eukaryotic Type C/Class 2 complex II molecule to be characterized, is composed of four protein subunits (Fig. 2A): hydrophilic Fp (residues A33–A645) and Ip (B33–B281) subunits, and membrane-anchoring hydrophobic CybL (C34–C186) and CybS (D28–D156) subunits [20]. Several terminal residues of each mature polypeptide (Fp: A31–A645, Ip: B29–B282, CybL: C32–C188 and CybS: D26–D156) are missing in the current model because of faint electron density. The enzyme accommodates five prosthetic groups: a FAD molecule, three ion-sulfur centers ([2Fe–2S], [4Fe–4S], [3Fe–4S]), and one heme *b* molecule (Fig. 2B). Although there are two molecules in the asymmetric unit, *A. suum* QFR, like *E. coli* QFR [18], porcine SQR [22] and chicken SQR [23], exists as a monomer both in solution and crystal, which distinguishes the enzyme from the reported dimer structure of *W. succinogenes* QFR [19] and the trimer structure of *E. coli* SQR [21]. Further, the amino acid sequence of each subunit of *A. suum* QFR (Fig. 3) shows higher identity with porcine and chicken SQRs than with *E. coli* SQR and *E. coli* and *W. succinogenes* QFRs. Accordingly, *A. suum* QFR is more closely related to porcine and chicken SQRs rather to *E. coli* and *W. succinogenes* bacterial complex IIs. The arrangement of the bound prosthetic groups in the *A. suum* QFR structure [20] is similar to that of other complex IIs with known structures [18,19,21–23]. The chain of the FAD, [2Fe–2S], [4Fe–4S] and [3Fe–4S] prosthetic groups is disposed between dicarboxylate- and quinone-binding sites with the distances between neighboring centers less than 14 Å (Fig. 2B), suggesting that electron transfer from RQH_2 to FAD is carried out by quantum tunneling [28], as proposed for *E. coli* SQR [21].

2.2. Fp subunit

The largest Fp subunit of *A. suum* QFR [20] folds into four domains (Fig. 4A): a FAD-binding domain (residues A33–A280 and A380–A465), a capping domain (A281–A379), a helical domain (A466–A568), and a C-terminal domain (A569–A645). The FAD molecule forms a covalent bond with His A79 and hydrogen bonds primarily with main-chain N atoms of highly conserved residues of the FAD-binding domain (A49, A71, A72, A73, A78, A80, A84, A85, A86, A201, A255, A421, A432, A437 and A438). In addition, residues within 5 Å of the FAD group, especially those close to the FAD isoalloxazine ring, are highly conserved (Fig. 3A).

Examination of the refined structure shows significant electron density near the isoalloxazine ring that can be assigned as malonate, an additive for crystallization [20]. The location of this site is in agreement with the dicarboxylate-binding site assigned to other complex IIs with known structures [18,19,21–23] and is constructed by residues of the FAD-binding domain (A84, A85, A153, A276, A387, A432 and A435) and the capping domain (A286, A288, A289 and A320). Three basic residues, Arg A320, His A387 and Arg A432, interact with the C3 carboxylate group of the bound malonate, and Thr A288 and Arg A320 with the C1 carboxylate group (Fig. 4A). With the exception of A84, A153 and A435, these residues are conserved across complex II molecules with known structures (Fig. 3A).

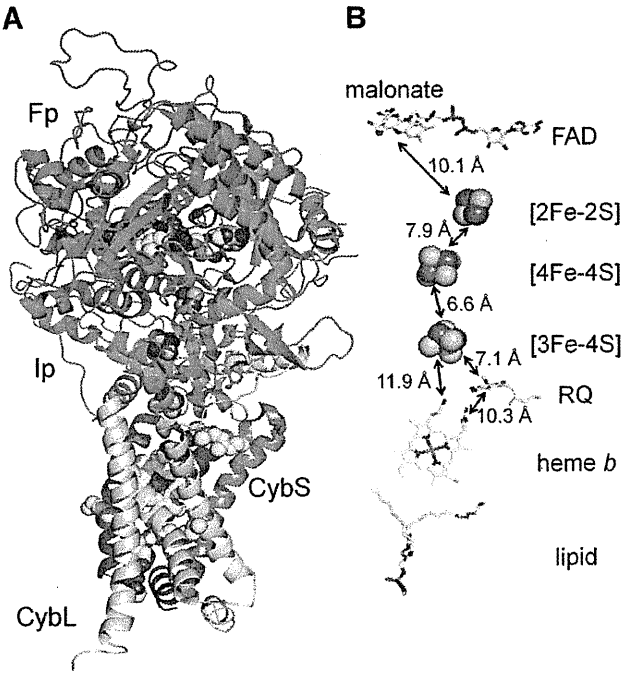

Fig. 2. Overall structure of *A. suum* QFR. (A) Cartoon representation of the overall structure of *A. suum* QFR. FAD-binding subunit (Fp) is shown in green; iron–sulfur subunit (Ip) is shown in cyan; and the transmembrane subunits CybL and CybS are shown in yellow and orange, respectively. The intrinsic redox centers (FAD, [2Fe–2S], [4Fe–4S], [3Fe–4S] and heme *b*) and bound small molecules (malonate, rhodoquinone, and lipid) are shown as spheres. (B) The arrangement of the redox centers together with malonate, rhodoquinone and lipid, and edge-to-edge distances between adjacent redox centers. For calculation of edge-to-edge distances, the dominant determinants of the electron tunneling rate, the sulfur atoms of the cysteine residues ligating to the iron–sulfur centers are included as part of the redox centers. The FAD edge is the isoalloxazine ring system and the heme edge is the conjugated macrocycle. Color-coding for each atom type is as follows: C, white; N, blue; O, red; S, dark yellow; and Fe, brown.

Please cite this article as: S. Harada, et al., Diversity of parasite complex II, Biochim. Biophys. Acta (2013), http://dx.doi.org/10.1016/j.bbabio.2013.01.005

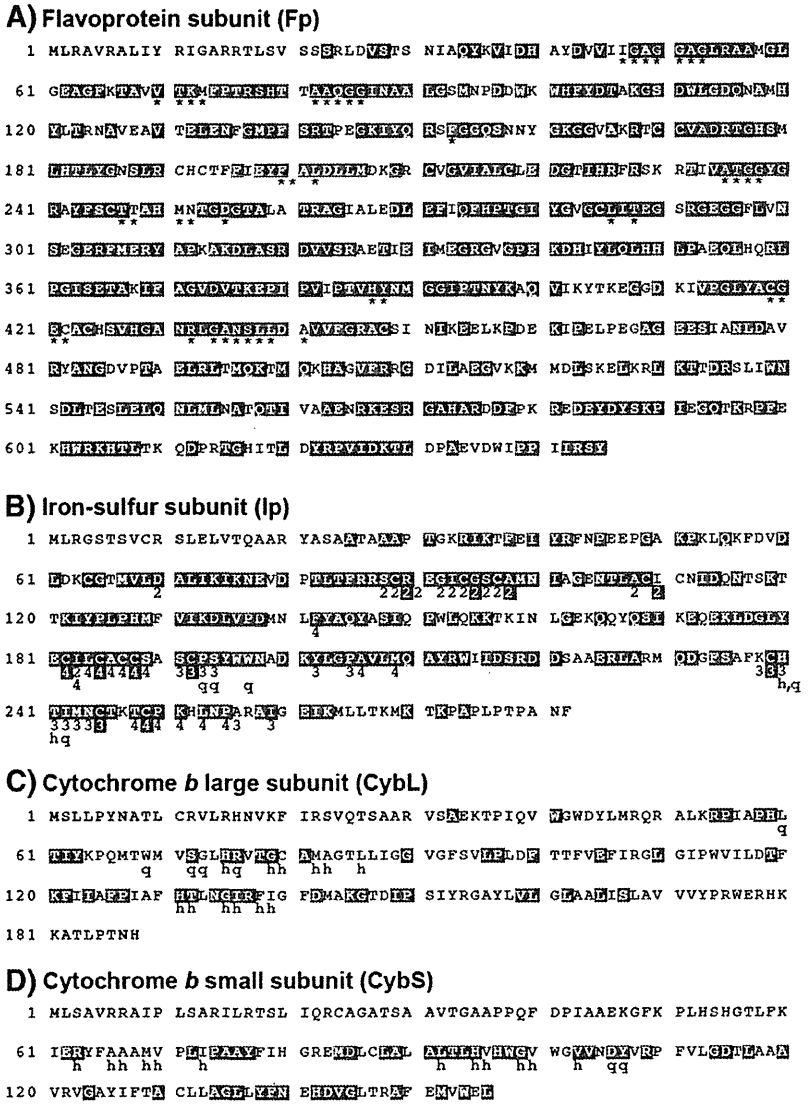

Fig. 3. Amino acid sequences of *A. suum* SQR. (A) Fp, (B) Ip, (C) CybL, and (D) CybS subunits. Residues conserved in the six complex II molecules with known structures (SQRs from porcine, chicken, and *E. coli* and QFRs from *E. coli*, *W. succinogenes*, and *A. suum*) are highlighted in red, residues conserved in SQRs from porcine, chicken, and *E. coli* and *A. suum* QFR are highlighted in green, residues conserved in porcine and chicken SQRs and *A. suum* QFR are highlighted in blue. Residues within 5 Å of FAD, [2Fe–2S], [4Fe–4S], [3Fe–4S], rhodoquinone and heme *b* redox centers are marked by *, 2, 4, 3, q, and h, respectively.

2.3. Ip subunit

The Ip subunit (Fig. 4B) is constructed by two domains, a plant ferredoxin-like N-terminal (B33–B130) and a bacterial ferredoxin-like C-terminal (B131–B281) domain [20]. The [2Fe–2S] center is bound to the N-terminal domain through coordination bonds with four cysteine residues (B89, B94, B97, and B109). The [4Fe–4S] and [3Fe–4S] centers are bound to the C-terminal domain and are coordinated by four (B182, B185, B188, and B249) and three (B192, B239, and B245) cysteine residues, respectively. Except for Cys B97, which is replaced by aspartate (Asp B63) in *E. coli* SQR [21], the cysteine residues are conserved (Fig. 3B). Out of 47 residues located within 5 Å of the iron–sulfur center of *A. suum* QFR [20], 44 residues are conserved in porcine and chicken SQRs, but that number decreases to 20 residues when compared across all complex II molecules with known structures [18,19,21–23]. The sulfur atoms of the cysteine ligands of [2Fe–2S] and [4Fe–4S] form –S:···H–N< interactions with main-chain amino groups of the N-terminal domain (B91, B92, B93, B96, and B108) and C-terminal domain (B184, B186, B187, B189, and B251), respectively. In addition, sulfur atoms of the iron–sulfur centers interact with the Ip subunit: the [2Fe–2S] center interacts with B90 N and B95 N, the [4Fe–4S] center with B183 N and B186 N, and the [3Fe–4S] center with B243 N. The –S:···H–N< interaction is also found in other complex II molecules [18, 19, 21–23, pdb code: 1L0V, 1QLB, 1NEK, 1ZOY and 1YQ3] and could affect the basicity of sulfur atoms of the cysteine ligands and the redox centers. It is worth noting that side chain atoms of Ser B96, Cys B187, and Tyr B202 interact with sulfur atoms of Cys B94, Cys B185, and [3Fe–4S], respectively (Fig. 4B). Although these residues are conserved in porcine and chicken complex II molecules (Fig. 3), Cys B187 is replaced by Leu in *E. coli* QFR, and Tyr B202 is replaced by Phe in *E. coli* and *W. succinogenes* QFRs and *E. coli* SQR. Therefore, *A. suum* QFR is more similar to mitochondrial porcine and chicken SQRs than bacterial complex II molecules with respect to the environment of the iron–sulfur centers.

Please cite this article as: S. Harada, et al., Diversity of parasite complex II, Biochim. Biophys. Acta (2013), http://dx.doi.org/10.1016/j.bbabio.2013.01.005

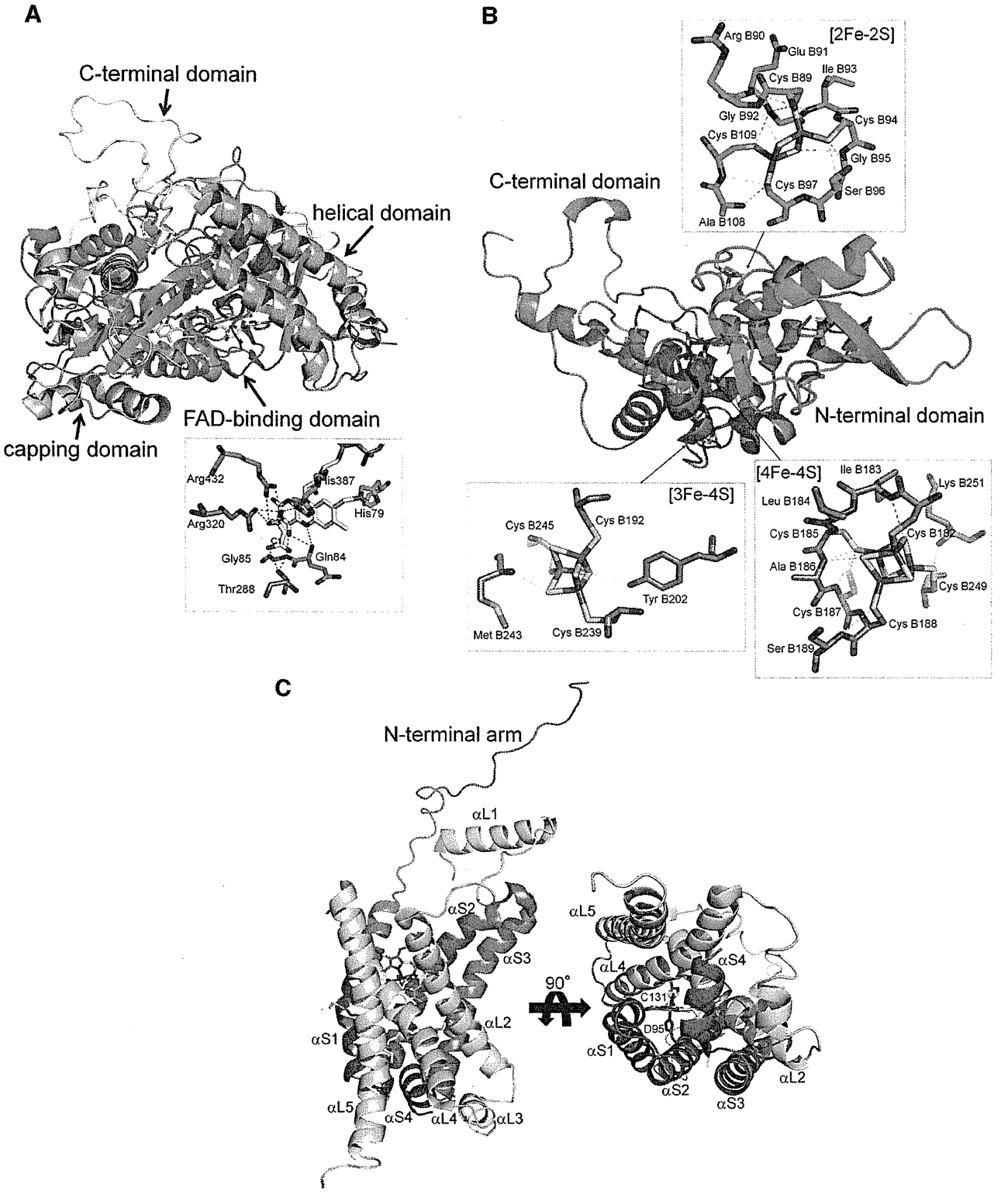

Fig. 4. Depiction of subunits. (A) Cartoon representation of the Fp subunit. The FAD-binding domain, capping domain, helical domain and C-terminal domain are shown in pale green, light blue, light pink and white, respectively, together with the stick models of FAD and malonate. The close-up view of the neighborhood of FAD is also represented in the inset. Color-coding for each atom type: C, white; N, blue; and O, red. Carbon atoms of residues from the FAD-binding domain and capping domain are shown in pale green and light blue, respectively. (B) Cartoon representation of the N-terminal domain (cyan) and C-terminal domain (light blue) of the Ip subunit together with the iron–sulfur centers shown as stick models. The close-up view of the iron–sulfur centers, cysteine ligands and residues interacting with the centers are shown in the insets. In (A) and (B), hydrogen bonds are shown with dashed lines. (C) Cartoon representation of the membrane-anchoring CybL (yellow) and CybS (orange) subunits together with heme *b* and the bound lipid molecule viewed from orientations perpendicular to each other. C131 and D95 are histidine residues from CybL and CybS subunits, respectively.

Please cite this article as: S. Harada, et al., Diversity of parasite complex II, Biochim. Biophys. Acta (2013), http://dx.doi.org/10.1016/j.bbabio.2013.01.005

2.4. Transmembrane CybL and CybS subunits

The membrane anchor of *A. suum* QFR, like *E. coli*, porcine and chicken SQRs [21–23], is made up of CybL and CybS subunits. They are composed of five (CybL: αL1–αL5) and four (CybS: αS1–αS4) α-helices, of which αL2, αL4, αL5, αS1, αS2, and αS3 are transmembrane helices [20]. Four helices, αL2, αL4, αS1, and αS2, form a helix bundle in which a heme *b* molecule is accommodated through ligation of conserved His C131 and His D95 (Fig. 4C). Unlike the FAD molecule and the iron–sulfur centers, most residues near the heme *b* molecule are not conserved (Fig. 3C and D). A lipid molecule is bound below the heme *b* site in the helix bundle. Phosphatidylethanolamine is incorporated into the current model, although electron density patterns are not clear enough to identify the lipid species. Both heme *b* and lipid molecules are located at the interface of CybL and CybS subunits and may contribute to the assembly of the CybL and CybS subunits. Interestingly, a segment comprising 27N-terminal residues (D28–D54, Fig. 4C) of the CybS subunit extends to the Fp and Ip subunits and five residues (D29, D39, D41, D42, D46) form inter-subunit hydrogen bonds with residues of Fp (A471, A195, A192) and Ip (B150). The segment is unique to *A. suum* QFR, and seems to contribute to the stabilization of the multi-subunit structure of the enzyme. A definite cleft is formed at the interface of the Ip, CybL, and CybS subunits, and residual electron density probably revealing a bound RQ molecule is found in the cleft. The location of the cleft is in agreement with the quinone-binding sites assigned in the structures of other complex II molecules [18,21–23]. In the refined structure (3VR8), RQ is well situated in the cleft (Fig. 2) and is surrounded by residues that are highly conserved among complex II molecules from porcine, chicken and *A. suum* (Fig. 3C and D).

2.5. Mechanisms of fumarate reduction and rhodoquinol oxidization

The crystal structure of the fumarate-bound *A. suum* QFR (3VRB) clearly reveals that a fumarate molecule is bound to the dicarboxylate site in a non-planar conformation (Fig. 5A); C2, C3, and C4 carboxyl groups are in the same plane parallel to the FAD isoalloxazine ring but the C1 carboxyl group deviates from the plane as indicated by a C3–C2–C1–O1A dihedral angle of 83.7°. The non-planar conformation is stabilized by hydrogen bonds with conserved residues; the C1 carboxyl group with Gly A85, His A276, Thr A288, and Glu A289, and the C4 carboxyl group with Arg A320, His A387, Arg A432, and Ala A435. Accordingly, the structure suggests that the uniform distribution of π-electrons over the conjugated double bonds of fumarate is disrupted and that a partial charge separation, $C2^{\delta+}$ and $C3^{\delta-}$, is induced on the bound fumarate molecule. This charge separation seems to be the key to the reduction of fumarate because the contact of $C2^{\delta+}$ with FAD N5 (3.5 Å) observed in the crystal structure should facilitate the hydride (or hydride equivalent) transfer from reduced FAD N5 to $C2^{\delta+}$. The twisted conformation of fumarate is also observed in *E. coli* [29] and *W. succinogenes* [19] QFRs, as well as in flavoproteins such as flavocytochrome *c* [30] and *T. cruzi* dihydroorotate dehydrogenase [31], and the similar mechanism of fumarate reduction has been proposed for these enzymes. The crystal structure also suggests that conserved Arg A320 probably supplies a proton to $C3^{\delta-}$ to complete the fumarate reduction.

Fig. 5B shows the RQ binding site of *A. suum* QFR. Of 12 residues within 5 Å of the bound RQ, nine residues (B193, B194, B197, B240, B242, C72, C76, D106, and D107) are conserved in porcine, chicken, and *E. coli* SQRs (Fig. 3). The [3Fe–4S] center, the nearest iron–sulfur center to the bound RQ, is located at distances of 9.1 and 7.7 Å from RQ O1 and O2, respectively, indicating that electrons are transferred from RQH_2 to FAD *via* the [3Fe–4S], [4Fe–4S], and [2Fe–2S] centers. Although residues surrounding heme *b* are mostly not conserved among complex II molecules (Fig. 3), the possibility of heme *b* to act as an electron acceptor from RQH_2 remains because heme *b* is also the redox center close to the bound RQ (Fig. 2B) and its redox potential (−34 mV, [16]) is higher than that of RQH_2 (−63 mV). RQ is also surrounded by conserved amino acid residues in SQRs from porcine, chicken and *E. coli* (Ser C72, Arg C76, Asp D106, and Tyr D107) and is involved in these hydrogen bond networks: RQ O1····Tyr D107····Arg C76····Asp D106 and RQ O2····Ser C72····RQ N····Arg C76····Asp D106. Protons abstracted from RQH_2 can leave along these networks. It should be noted that the amino group of RQ, which is replaced by the methoxy group in ubiquinone, is involved in one of the hydrogen bond networks.

2.6. Flutolanil-binding site

In both crystal structures of *A. suum* QFR (Fig. 6A, 3VRB) and porcine SQR (Fig. 6B, 3AE8) complexed with flutolanil, an inhibitor specific for *A. suum* QFR [26], flutolanil is bound to the quinone-binding site located near the [3Fe–4S] center (Q_p site), where residues of *A. suum* QFR and porcine SQR within 5 Å of the bound flutolanil are mostly identical (73%). The isopropoxy-phenyl moiety of flutolanil comes in contact with conserved hydrophobic residues and the carbonyl oxygen forms hydrogen bonds with tyrosine and tryptophan residues. Accordingly, these hydrogen bonds as well as van der Waals contact seem to be important for the binding of flutolanil to both enzymes. It is worth noting that there is close contact between the isopropoxy group of the bound flutolanil and the aromatic indole ring of *A. suum* QFR Trp C69; these are separated by 3.3 Å, significantly less than the distance expected for van der Waals contact (3.7 Å), indicating that they interact with each other through a C–H····π interaction. Since the tryptophan residue is replaced by methionine (Met C39) in porcine SQR, this electrostatic interaction is unique to *A. suum* QFR. Another electrostatic interaction unique to *A. suum* QFR is formed between the flutolanil trifluoromethylbenzene moiety and Arg C76 guanidino group. Since the trifluoromethyl group is an electron-withdrawing group, the π-orbital of the flutolanil aromatic ring is expected to be deficient in electrons. In contrast, the π-orbital of the guanidino group of Arg C76 seems to be rich in electrons because the arginine residue located in the hydrophobic environment of the membrane-anchoring CybL subunit may preferentially the unprotonated form over the protonated one. Therefore, the stacking of the two π-orbitals, one is deficient and another rich in electron, with the distance of 3.2 Å observed in the *A. suum* QFR-flutolanil complex reinforce the attractive interaction between flutolanil and *A. suum* QFR. In porcine SQR, however, the guanidino group of Arg C46, the counterpart residue to Arg C76, is a greater distance from the flutolanil trifluoromethylbenzene moiety and is poorly stacked.

In contrast to flutolanil, 2-thenoyltrifluoroacetone (TTFA), a potent inhibitor against mammalian SQR, does not inhibit both *A. suum* QFR and SQR [11]. There are two TTFA binding sites in porcine SQR [22], Q_p and Q_d sites. The Q_p site TTFA, like flutolanil bound to the Q_p site, accepts hydrogen bonds and van der Waals contacts from residues that, except for Trp C35 (Pro C65 in *A. suum* enzymes), are conserved in the *A. suum* enzymes, whereas the Q_d site TTFA is surrounded mostly by residues unconserved in the *A. suum* enzymes and interacts with porcine SQR mainly through water molecules [22]. Therefore, if it is assumed that the Q_p site is more crucial for the inhibition of complex II than the Q_d site, the insensitivity of *A. suum* enzymes toward TTFA may be caused by the change from Trp C35 to Pro C65.

3. Twelve novel subunits of *T. cruzi* complex II

3.1. Subunit structure of T. cruzi complex II

The parasitic protist *T. cruzi* is the etiological agent of Chagas disease, a public health threat in Central and South America. These parasites are normally transmitted by the reduviid bug *via* vector feces after a bug bite and are also transferred *via* transfusion of infected

Please cite this article as: S. Harada, et al., Diversity of parasite complex II, Biochim. Biophys. Acta (2013), http://dx.doi.org/10.1016/j.bbabio.2013.01.005

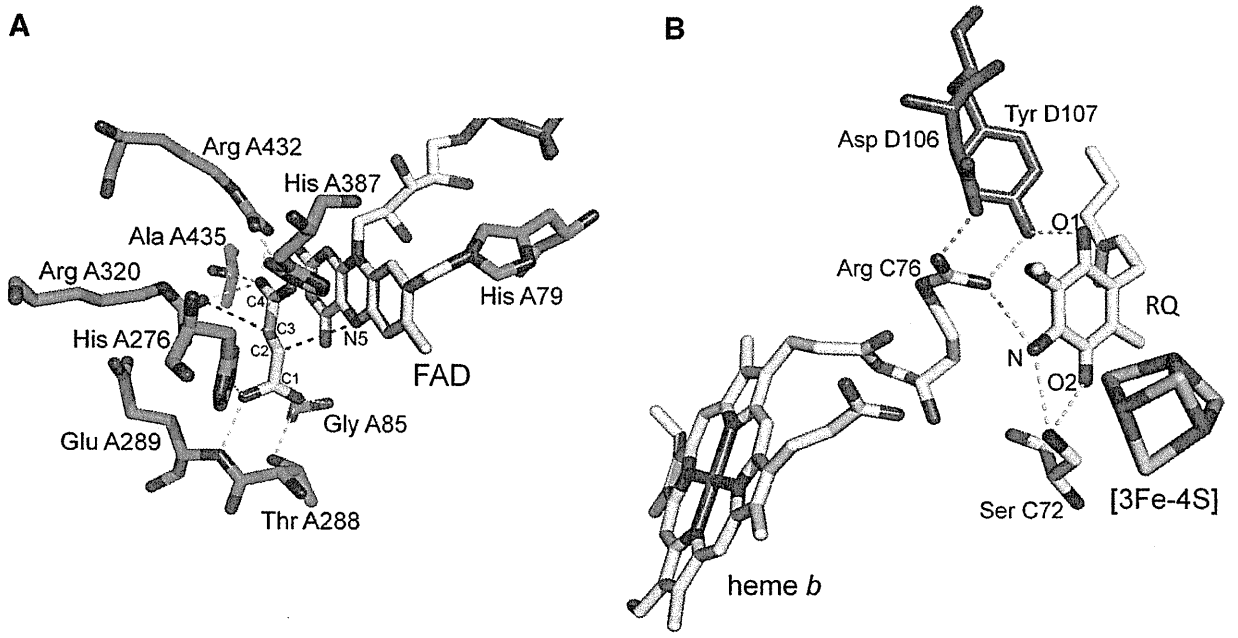

Fig. 5. Close-up view of active site structures. (A) The fumarate molecule bound to the dicarboxylate-binding site of *A. suum* QFR and residues interact with fumarate. Hydrogen bonds are shown in yellow dashed lines. Red dashed lines indicate probable routes of hydride (FAD N5→fumarate $C2^{\delta+}$) and proton (Arg A320 $N\eta_1 \rightarrow C3^{\delta-}$) transfers to reduce fumarate. (B) Rhodoquinol binding site of *A. suum* QFR. Hydrogen bonds are shown in yellow dashed lines. Color-coding for each atom type is as follows: N, blue; O, red; S, dark yellow; and Fe, brown. Carbon atoms of FAD, RQ and heme *b* are shown in white, residues from Fp, CybL and CybS are shown in light green, yellow, and orange, respectively.

blood. About 16 to 18 million people are infected and 100 million are at risk, but there are no definitive chemotherapeutic treatments available [32].

To our surprise, the complex II purified from *T. cruzi* consists of six hydrophilic (SDH1, $SDH2_N$, $SDH2_C$, and SDH5–SDH7) and six hydrophobic (SDH3, SDH4, and SDH8–SDH11) nuclear-encoded subunits (Fig. 7; [24]). SDH1 and SDH2 correspond to Fp (SDHA) and Ip (SDHB), respectively. Orthologous genes for each subunit were identified in most trypanosomatids, including *T. brucei* and *Leishmania major* [33–35]. Notably, the iron–sulfur subunit was heterodimeric; $SDHB_N$ and $SDHB_C$ contain the plant-type ferredoxin domain in the N-terminal half and the bacterial ferredoxin domain in the C-terminal half, respectively. Catalytic subunits (SDHA, $SDHB_N$ *plus* $SDHB_C$, SDH3, and SDH4) contain all key residues for binding of dicarboxylates and quinones, but the enzyme showed lower affinity for both substrates and inhibitors than mammalian enzymes. In addition, the enzyme binds protoheme IX, but SDH3 lacks a histidine ligand [24].

3.2. Split Ip subunit of Trypanosomal complex II

In contrast to the monomeric iron–sulfur subunit (SDHB) found in all known families of complex II, the Trypanosomal iron–sulfur subunit is composed of two nuclear-encoded genes for $SDHB_N$ and $SDHB_C$ subunits (Fig. 7) [24]. The crystal structure of the Ip subunit from porcine complex II [22] and the PHYRE^2 model [36] of *T. cruzi* $SDHB_N$ (residues B_N66 to B_N161) and $SDHB_C$ (residues B_C34 to B_C163) are shown in Fig. 8A and B, respectively. The C-terminal extension of $TcSDHB_N$ (residues B_N162 to B_N270) was removed from the model to allow better comparison between porcine Ip (Fig. 8A) and split Trypanosomal Ip (Fig. 8B) subunits. According to this model, the [2Fe–2S] center is bound to the $TcSDHB_N$ subunit (Fig. 8B) by four cysteine residues, B_N120, B_N125, B_N128, and B_N140 (Fig. 9), which correspond to cysteine residues B65, B70, B73, and B85 from porcine SDHB [22]. The [4Fe–4S] center is bound to $TcSDHB_C$ by cysteine residues B_C71, B_C74, B_C77, and B_C138 (Fig. 9), which correspond to cysteine residues B158, B161, B164, and B225 from the porcine SDHB subunit and, finally, the [3Fe–4S] center is bound by cysteine residues B_C81, B_C128, and B_C134 (Fig. 9), which correspond to cysteine residues B168, B215, and B221 from porcine SDHB subunit [22]. The residues from SDHB subunit which interact with flutolanil from porcine complex II (B216, B218, B169, and B173 from Fig. 4B) are also found in $TcSDHB_C$ (B_C82, B_C86, B_C129, and B_C131 in Fig. 9). Thus, even if the Ip subunit of the Trypanosomatid complex II is comprised of two distinct peptides, the three iron–sulfur clusters as well as all cysteine residues necessary to bind those clusters are structurally conserved among all families of complex II. Such spatial organization of iron–sulfur clusters is expected to be crucial for optimal electron transfer from succinate to ubiquinone.

3.3. T. cruzi complex II as a drug target

Purified *T. cruzi* enzyme shows reduced binding affinities for both substrates and inhibitors. Its K_m values for ubiquinone (18.8 ± 6.4 μM (Q_2)) and succinate (1.48 ± 0.17 mM) were higher than those with bovine enzyme [37] (0.3 and 130 μM, respectively) and *E. coli* enzyme [38,13] (2 and 277 μM, respectively). Interestingly, the *T. cruzi* enzyme K_m value for succinate was comparable to 610 μM in adult *A. suum* [10], which expresses the stage-specific complex II as QFR under hypoxic environments in the host organisms mentioned above.

Sensitivity to inhibitors also differs from that of other complex II molecules. Atpenin A5, a potent inhibitor for complex II, inhibited the *T. cruzi* enzyme with an IC_{50} value of 6.4 ± 2.4 μM, which is three orders of magnitude higher than that of bovine enzyme (4 nM) [39]. Furthermore, *T. cruzi* enzyme does not respond to carboxin, 2-theonyltrifluoroacetone (TTFA), plumbagin, and 2-heptyl-4-hydroxyquinoline N-oxide (HQNO) (100 μM$<IC_{50}$). Structural divergence in Trypanosomatid SDH3 and SDH4 could be the cause for lower binding affinities for both quinones and inhibitors. In addition, the IC_{50} for malonate (40 μM) was much higher than the K_i value for bovine complex II (1.3 μM) [37], indicating different structures of the dicarboxylate-binding site.

These unusual features are unique in Trypanosomatidae and make their complex II molecules a target for new chemotherapeutic agents. Insensitivity to a known inhibitor is a promising feature for identifying a specific and potent inhibitor. Ascofuranone, which is a most

Please cite this article as: S. Harada, et al., Diversity of parasite complex II, Biochim. Biophys. Acta (2013), http://dx.doi.org/10.1016/j.bbabio.2013.01.005

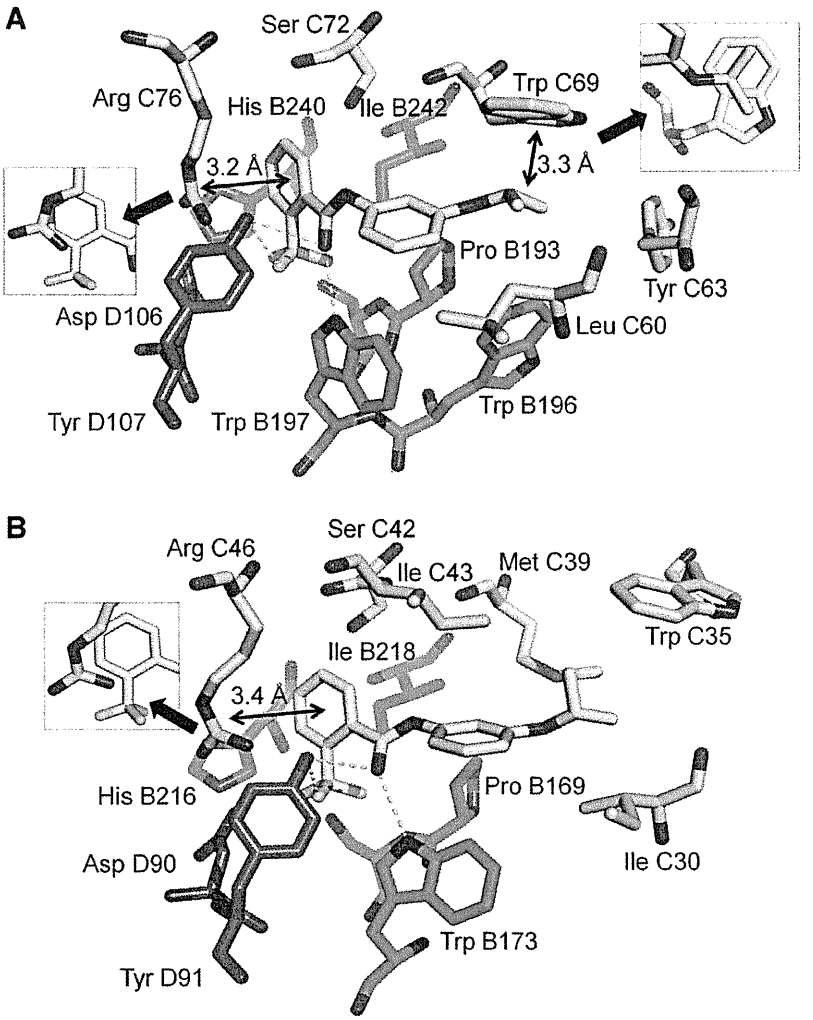

Fig. 6. Flutolanil binding site. The structures of flutolanil binding sites of (A) *A. suum* QFR and (B) porcine SQR. In each structure, the flutolanil molecule is bound to the quinone-binding site and surrounded by residues from Ip (cyan), CybL (yellow), and CybS (orange) subunits. Most of these residues are conserved between the two enzymes. Close-up views of the C—H·····π interaction between the isopropoxy group of flutolanil and Trp C69 side chain, and the electrostatic interaction between the flutolanil trifluoromethylbenzene moiety and Arg C76 guanidino group are shown in insets. Hydrogen bonds are shown in yellow dashed lines.

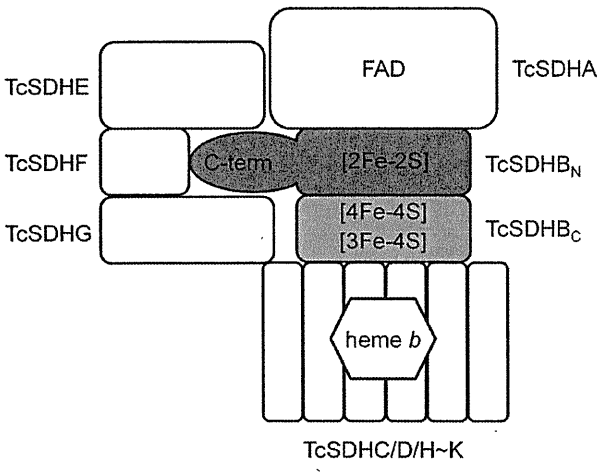

Fig. 7. Subunit organization model of Trypanosomal complex II. The Trypanosomal complex II is composed of six hydrophilic subunits (SDHA/B_N/B_C/E–G) and six hydrophobic subunits (SDHC/D/H–K). In the case of Trypanosomal complex II, the canonical SDHB is split into $SDHB_N$ (pink) and $SDHB_C$ (blue).

potent inhibitor of cyanide-insensitive alternative oxidase of *T. brucei* is good example [40].

4. Perspectives and conclusion

As described above, parasites have exploited a variety of energy-transducing systems in their adaptation to specific environments inside their hosts. Dynamic rearrangement of the respiratory chain during the life cycle is one of the key elements of this adaptation. However, the control mechanism responsible for stage-specific expression of the genes of parasites remains unclear because research on parasites at the molecular level has only recently begun. In this regard, recent reports indicating that complex II functions as an oxygen sensor are of great interest [41]. Mammalian cells are able to sense decreased oxygen availability and activate response systems, including transcriptional activation of several genes controlled via hypoxia-inducible factor-1 (HIF-1) [42]. Although the molecular mechanism of gene expression has not been elucidated for parasites, *A. suum* shows a very clear transition of the metabolic systems between larvae and adult stages, and it is, thus, a very promising research model. Our recent results show that a HIF-1 homologue plays a role in oxygen adaptation in *A. suum* and sequence analysis

Please cite this article as: S. Harada, et al., Diversity of parasite complex II, Biochim. Biophys. Acta (2013), http://dx.doi.org/10.1016/j.bbabio.2013.01.005

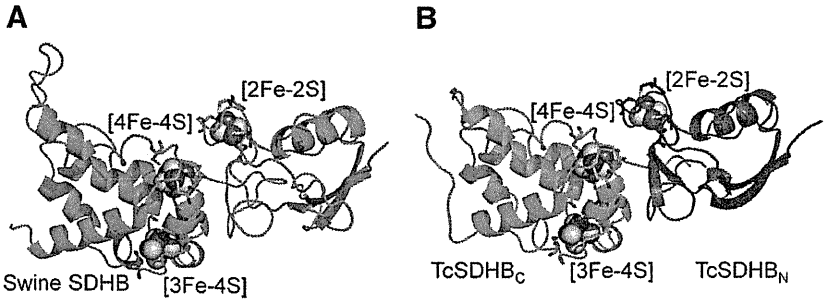

Fig. 8. PHYRE^2 model of split *T. cruzi* SDHB subunits. Superposition of porcine SDHB crystal structure (green, residues Pro B9 to Glu B237) (A), with the PHYRE^2 model of *T. cruzi* SDHB$_N$ (pink, residues Thr B$_N$66 to Asp B$_N$161) and SDHB$_C$ (blue, residues Val B$_C$34 to Pro B$_C$163) subunits (B). All cysteine residues coordinating with the Fe–S clusters are conserved and represented as stick, while iron (orange) and sulfur (yellow) clusters as spheres. The C-terminal residues from B$_N$162 to B$_N$270 of TcSDHB$_N$ were removed from the PHYRE^2 model for ease of comparison between porcine and *T. cruzi* SDHB subunits.

of the 5′-upstream regions of complex II genes identified putative hypoxia-responsive element (HREs), suggesting that HIF-1 directly regulates the expression of stage-specific complex II isoforms [43].

Diversity of complex II is found not only in parasites but also in human host. Two isoforms of human Fp, type I and type II, were reported [44,45]. These isoforms differed from each other only in two amino acid residues: Tyr 586 and Val 614 of type I Fp are replaced by Phe 586 and Ile 614 in type II Fp, respectively. Type I Fp are well conserved among the Fp of mammals, and type II Fp is found only in human complex II. Although the type I Fp gene is located on chromosome 5p15 and has an exon–intron structure [44,46], the type II Fp gene is not found in the NCBI database. Baysal et al. suggested that type II Fp is a variant of the Fp subunit and can be explained by balancing selection over the long term [47]. Interestingly, expression of type II Fp mRNA is increased in normal cells cultured under ischemic conditions [48]. It is of interest to speculate that complex II^{II} has higher QFR activity and plays an important role in fumarate respiration in human mitochondria as the terminal oxidase of the system similar to that in *A. suum* adult complex II. Anti-cancer activity of pyrvinium pamoate an anthelmintic, which is a known fumarate reductase inhibitor, against human cancer cells should be studied further [49]. The diversity of mitochondrial complex II molecules lends itself to studies in many areas, including bioenergetics, molecular evolution and drug discovery.

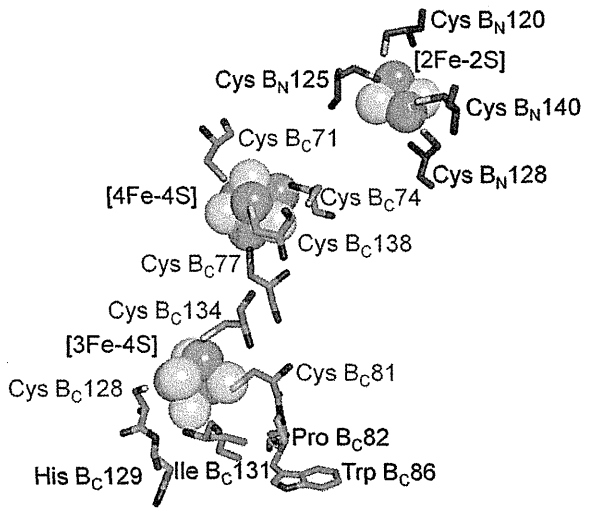

Fig. 9. All cysteines necessary for binding Fe–S clusters are conserved in Trypanosomal split Ip subunits. Cysteine residues from SDHB$_N$ are colored and labeled in pink and residues from SDHB$_C$ are in blue. The equivalent residues from Trypanosomal SDHB$_C$, which were found to interact with flutolanil from porcine SDHB are labeled in red. The three iron (orange) and sulfur (yellow) clusters are represented as spheres.

Acknowledgments

This work was supported in part by Programme for the Promotion of Basic and Applied Researches for Innovations in Bio-oriented Industry (BRAIN), a Creative Scientific Research Grant 18GS0314, a Grant-in-Aid for Scientific Research on Priority Areas 18073004 from the Japanese Society for the Promotion of Science, and the Targeted Proteins Research Program of the Japanese Ministry of Education, Science, Culture, Sports and Technology (MEXT).

References

[1] K. Kita, H. Hirawake, S. Takamiya, Cytochromes in the respiratory chain of helminth mitochondria, Int. J. Parasitol. 27 (1997) 617–630.
[2] R. Komuniecki, P.R. Komuniecki, Aerobic–anaerobic transitions in energy metabolism during the development of the parasitic nematode *Ascaris suum*, in: J.C. Boothroyd, R. Komuniecki (Eds.), Molecular Approaches to Parasitology, Wiley-Liss, Inc., New York, 1995, pp. 109–121.
[3] A.G.M. Tielens, C. Rotte, J.J. van Hellemond, W. Martin, Mitochondria as we don't know them, Trends Biochem. Sci. 27 (2002) 56–72.
[4] K. Kita, S. Takamiya, Electron-transfer complexes in *Ascaris* mitochondria, Adv. Parasitol. 51 (2002) 95–131.
[5] K. Kita, Electron-transfer complexes in *Ascaris suum*, Parasitol. Today 8 (1992) 155–159.
[6] H. Amino, A. Osanai, H. Miyadera, N. Shinjyo, E. Tomitsuka, H. Taka, R. Mineki, K. Murayama, S. Takamiya, T. Aoki, H. Miyoshi, K. Sakamoto, S. Kojima, K. Kita, Isolation and characterization of the stage-specific cytochrome *b* small subunit (CybS) of *Ascaris suum* complex II from the aerobic respiratory chain of larval mitochondria, Mol. Biochem. Parasitol. 128 (2003) 175–186.
[7] H. Amino, H. Wang, H. Hirawake, F. Saruta, D. Mizuchi, R. Mineki, N. Shindo, K. Murayama, S. Takamiya, T. Aoki, S. Kojima, K. Kita, Stage specific isoforms of *Ascaris suum* complex II: the fumarate reductase of the parasitic adult and the succinate dehydrogenase of free-living larvae share a common iron–sulfur subunit, Mol. Biochem. Parasitol. 106 (2000) 63–76.
[8] K. Kita, H. Hirawake, H. Miyadera, H. Amino, S. Takeo, Role of complex II in anaerobic respiration of the parasite mitochondria from *Ascaris suum* and *Plasmodium falciparum*, Biochim. Biophys. Acta 1553 (2002) 123–139.
[9] S. Omura, H. Miyadera, H. Ui, K. Shiomi, Y. Yamaguchi, R. Masuma, T. Nagamitsu, D. Takano, T. Sunazuka, A. Harder, H. Kölbl, M. Namikoshi, H. Miyoshi, K. Sakamoto, K. Kita, An anthelmintic compound, nafuredin, shows selective inhibition of complex I in helminth mitochondria, Proc. Natl. Acad. Sci. U. S. A. 98 (2001) 60–62.
[10] F. Saruta, T. Kuramochi, K. Nakamura, S. Takamiya, Y. Yu, T. Aoki, K. Sekimizu, S. Kojima, K. Kita, Stage-specific isoforms of complex II (succinate–ubiquinone oxidoreductase) in mitochondria from the parasitic nematode, *Ascaris suum*, J. Biol. Chem. 270 (1995) 928–932.
[11] S. Takamiya, K. Kita, H. Wang, P.P. Weinstein, A. Hiraishi, H. Oya, T. Aoki, Developmental changes in the respiratory chain of *Ascaris* mitochondria, Biochim. Biophys. Acta 1141 (1993) 65–74.
[12] S.T. Cole, C. Condon, B.D. Lemire, J.H. Weiner, Molecular biology, biochemistry and bioenergetics of fumarate reductase, a complex membrane-bound iron–sulfur flavoenzyme of *Escherichia coli*, Biochim. Biophys. Acta 811 (1985) 381–403.
[13] H. Miyadera, A. Hiraishi, H. Miyoshi, K. Sakamoto, R. Mineki, K. Murayama, K.V. Nagashima, K. Matsuura, S. Kojima, K. Kita, Complex II from phototrophic purple bacterium *Rhodoferax fermentans* displays rhodoquinol–fumarate reductase activity, Eur. J. Biochem. 270 (2003) 1863–1874.

Please cite this article as: S. Harada, et al., Diversity of parasite complex II, Biochim. Biophys. Acta (2013), http://dx.doi.org/10.1016/j.bbabio.2013.01.005

[14] M. Heinz, Encyclopedic Reference of Parasitology, second ed. Springer, Berlin 2001.
[15] F. Iwata, N. Shinjyo, H. Amino, K. Sakamoto, M.K. Islam, N. Tsuji, K. Kita, Change of subunit composition of mitochondrial complex II (succinate-ubiquinone reductase/quinol-fumarate reductase) in *Ascaris suum* during migration in the experimental host, Parasitol. Int. 57 (2008) 54–61.
[16] C. Hägerhäll, Succinate: quinone oxidoreductases: variations on a conserved theme, Biochim. Biophys. Acta 1320 (1997) 107–141.
[17] R.S. Lemos, A.S. Fernandes, M.M. Pereira, C.M. Gomes, M. Teixeira, Quinol:fumarate oxidoreductases and succinate:quinone oxidoreductase: phylogenetic relationships, metal centres and membrane attachment, Biochim. Biophys. Acta 1553 (2002) 158–170.
[18] T.M. Iverson, C. Luna-Chavez, G. Cecchini, D.C. Rees, Structure of the *Escherichia coli* fumarate reductase respiratory complex, Science 284 (1999) 1961–1966.
[19] C.R.D. Lancaster, A. Kröger, M. Auer, H. Michel, Structure of fumarate reductase from *Wolinella succinogenes* at 2.2 Å resolution, Nature 402 (1999) 377–385.
[20] H. Shimizu, A. Osanai, K. Sakamoto, D.K. Inaoka, T. Shiba, S. Harada, K. Kita, Crystal structure of mitochondrial quinol–fumarate reductase from the parasitic nematode *Ascaris suum*, J. Biochem. 151 (2012) 589–592.
[21] V. Yankovskaya, R. Horsefield, S. Törnroth, C. Luna-Chavez, H. Miyoshi, C. Léger, B. Byrne, G. Cecchini, S. Iwata, Architecture of succinate dehydrogenase and reactive oxygen species generation, Science 299 (2003) 700–704.
[22] F. Sun, X. Huo, Y. Zhai, A. Wang, J. Xu, D. Su, M. Bartlam, Z. Rao, Crystal structure of mitochondrial respiratory membrane protein complex II, Cell 121 (2005) 1043–1057.
[23] L. Huang, G. Sun, D. Cobessi, A.C. Wang, J.T. Shen, E.Y. Tung, V.E. Anderson, E.A. Berry, 3-Nitropropionic acid is a suicide inhibitor of mitochondrial respiration that, upon oxidation by complex II, forms a covalent adduct with a catalytic base arginine in the active site of the enzyme, J. Biol. Chem. 281 (2006) 5965–5972.
[24] J. Morales, T. Mogi, S. Mineki, E. Takashima, R. Mineki, H. Hirawake, K. Sakamoto, S. Ōmura, K. Kita, Novel mitochondrial complex II isolated from *Trypanosoma cruzi* is composed of twelve peptides including a heterodimeric Ip subunit, J. Biol. Chem. 284 (2009) 7255–7263.
[25] T. Mogi, K. Kita, Identification of mitochondrial complex II subunits SDH3 and SDH4 and ATP synthase subunits a and b in *Plasmodium* spp, Mitochondrion 9 (2009) 443–453.
[26] A. Osanai, S. Harada, K. Sakamoto, H. Shimizu, D.K. Inaoka, K. Kita, Crystallization of mitochondrial rhodoquinol-fumarate reductase from the parasitic nematode *Ascaris suum* with the specific inhibitor flutolanil, Acta Crystallogr., Sect. F: Struct. Biol. Cryst. Commun. 65 (2009) 941–944.
[27] K. Motoba, M. Uchida, E. Tada, Mode of antifungal action and selectivity of flutolanil, Agric. Biol. Chem. 52 (1988) 1445–1449.
[28] C.C. Page, C.C. Moser, X. Chen, P.L. Dutton, Natural engineering principles of electron tunnelling in biological oxidation-reduction, Nature 402 (1999) 47–52.
[29] T.M. Tomasiak, T.L. Archuleta, J. Andrell, C. Luna-Chavez, T.A. Davis, M. Sarwar, A.J. Ham, W.H. McDonald, V. Yankovskaya, H.A. Stern, J.N. Johnston, E. Maklashina, G. Cecchini, T.M. Iverson, Geometric restraint drives on- and off-pathway catalysis by the *Escherichia coli* menaquinol:fumarate reductase, J. Biol. Chem. 286 (2011) 3047–3056.
[30] P. Taylor, S.L. Pealing, G.A. Reid, S.K. Chapman, M.D. Walkinshaw, Structural and mechanistic mapping of a unique fumarate reductase, Nat. Struct. Biol. 6 (1999) 1108–1112.
[31] D.K. Inaoka, K. Sakamoto, H. Shimizu, T. Shiba, G. Kurisu, T. Nara, T. Aoki, K. Kita, S. Harada, Structures of *Trypanosoma cruzi* dihydroorotate dehydrogenase complexed with substrates and products: atomic resolution insights into mechanisms of dihydroorotate oxidation and fumarate reduction, Biochemistry 47 (2008) 10881–10891.
[32] World Health Organization Report of the first meeting of WHO Strategic and Technical Advisory Group on Neglected Tropical Diseases, WHO, Geneva, Switzerland, 2007.
[33] N.M. El-Sayed, P.J. Myler, D.C. Bartholomeu, D. Nilsson, G. Aggarwal, A.N. Tran, E. Ghedin, E.A. Worthey, A.L. Delcher, G. Blandin, S.J. Westenberger, E. Caler, G.C. Cerqueira, C. Branche, B. Haas, A. Anupama, E. Arner, L. Aslund, P. Attipoe, E. Bontempi, F. Bringaud, P. Burton, E. Cadag, D.A. Campbell, M. Carrington, J. Crabtree, H. Darban, J.F. da Silveira, P. de Jong, K. Edwards, P.T. Englund, G. Fazelina, T. Feldblyum, M. Ferella, A.C. Frasch, K. Gull, D. Horn, L. Hou, Y. Huang, E. Kindlund, M. Klingbeil, S. Kluge, H. Koo, D. Lacerda, M.J. Levin, H. Lorenzi, T. Louie, C.R. Machado, R. McCulloch, A. McKenna, Y. Mizuno, J.C. Mottram, S. Nelson, S. Ochaya, K. Osoegawa, G. Pai, M. Parsons, M. Pentony, U. Pettersson, M. Pop, J.L. Ramirez, J. Rinta, L. Robertson, S.L. Salzberg, D.O. Sanchez, A. Seyler, R. Sharma, J. Shetty, A.J. Simpson, E. Sisk, M.T. Tammi, R. Tarleton, S. Teixeira, S. Van Aken, C. Vogt, P.N. Ward, B. Wickstead, J. Wortman, O. White, C.M. Fraser, K.D. Stuart, B. Andersson, The genome sequence of *Trypanosoma cruzi*, etiologic agent of Chagas disease, Science 309 (2005) 409–415.
[34] M. Berriman, E. Ghedin, C. Hertz-Fowler, G. Blandin, H. Renauld, D.C. Bartholomeu, N.J. Lennard, E. Caler, N.E. Hamlin, B. Haas, U. Böhme, L. Hannick, M.A. Aslett, J. Shallom, L. Marcello, L. Hou, B. Wickstead, U.C. Alsmark, C. Arrowsmith, R.J. Atkin, A.J. Barron, F. Bringaud, K. Brooks, M. Carrington, I. Cherevach, T.J. Chillingworth, C. Churcher, L.N. Clark, C.H. Corton, A. Cronin, R.M. Davies, J. Doggett, A. Djikeng, T. Feldblyum, M.C. Field, A. Fraser, I. Goodhead, Z. Hance, D. Harper, B.R. Harris, H. Hauser, J. Hostetler, A. Ivens, K. Jagels, D. Johnson, J. Johnson, K. Jones, A.X. Kerhornou, H. Koo, N. Larke, S. Landfear, C. Larkin, V. Leech, A. Line, A. Lord, A. Macleod, P.J. Mooney, S. Moule, D.M. Martin, G.W. Morgan, K. Mungall, H. Norbertczak, D. Ormond, G. Pai, C.S. Peacock, J. Peterson, M.A. Quail, E. Rabbinowitsch, M.A. Rajandream, C. Reitter, S.L. Salzberg, M. Sanders, S. Schobel, S. Sharp, M. Simmonds, A.J. Simpson, L. Tallon, C.M. Turner, A. Tait, A.R. Tivey, S. Van Aken, D. Walker, D. Wanless, S. Wang, B. White, O. White, S. Whitehead, J. Woodward, J. Wortman, M.D. Adams, T.M. Embley, K. Gull, E. Ullu, J.D. Barry, A.H. Fairlamb, F. Opperdoes, B.G. Barrell, J.E. Donelson, N. Hall, C.M. Fraser, S.E. Melville, N.M. El-Sayed, The genome of the African trypanosome *Trypanosoma brucei*, Science 309 (2005) 416–422.
[35] A.C. Ivens, C.S. Peacock, E.A. Worthey, L. Murphy, G. Aggarwal, M. Berriman, E. Sisk, M.A. Rajandream, E. Adlem, R. Aert, A. Anupama, Z. Apostolou, P. Attipoe, N. Bason, C. Bauser, A. Beck, S.M. Beverley, G. Bianchettin, K. Borzym, G. Bothe, C.V. Bruschi, M. Collins, E. Cadag, L. Ciarloni, C. Clayton, R.M. Coulson, A. Cronin, A.K. Cruz, R.M. Davies, J. De Gaudenzi, D.E. Dobson, A. Duesterhoeft, G. Fazelina, N. Fosker, A.C. Frasch, A. Fraser, M. Fuchs, C. Gabel, A. Goble, A. Goffeau, D. Harris, C. Hertz-Fowler, H. Hilbert, D. Horn, Y. Huang, S. Klages, A. Knights, M. Kube, N. Larke, L. Litvin, A. Lord, T. Louie, M. Marra, D. Masuy, K. Matthews, S. Michaeli, J.C. Mottram, S. Müller-Auer, H. Munden, S. Nelson, H. Norbertczak, K. Oliver, S. O'neil, M. Pentony, T.M. Pohl, C. Price, B. Purnelle, M.A. Quail, E. Rabbinowitsch, R. Reinhardt, M. Rieger, J. Rinta, J. Robben, L. Robertson, J.C. Ruiz, S. Rutter, D. Saunders, M. Schäfer, J. Schein, D.C. Schwartz, K. Seeger, A. Seyler, S. Sharp, H. Shin, D. Sivam, R. Squares, S. Squares, V. Tosato, C. Vogt, G. Volckaert, R. Wambutt, T. Warren, H. Wedler, J. Woodward, S. Zhou, W. Zimmermann, D.F. Smith, J.M. Blackwell, K.D. Stuart, B. Barrell, P.J. Myler, The genome of the kinetoplastid parasite, *Leishmania major*, Science 309 (2005) 436–442.
[36] L.A. Kelley, M.J. Sternberg, Protein structure prediction on the Web: a case study using the Phyre server, Nat. Protoc. 4 (2009) 363–371.
[37] V.G. Grivennikova, E.V. Gavrikova, A.A. Timoshin, A.D. Vinogradov, Fumarate reductase activity of bovine heart succinate-ubiquinone reductase. New assay system and overall properties of the reaction, Biochim. Biophys. Acta 1140 (1993) 282–292.
[38] E. Maklashina, G. Cecchini, Comparison of catalytic activity and inhibitors of quinone reactions of succinate dehydrogenase (Succinate-ubiquinone oxidoreductase) and fumarate reductase (Menaquinol-fumarate oxidoreductase) from *Escherichia coli*, Arch. Biochem. Biophys. 369 (1999) 223–232.
[39] H. Miyadera, K. Shiomi, H. Ui, Y. Yamaguchi, R. Masuma, H. Tomoda, H. Miyoshi, A. Osanai, K. Kita, S. Omura, Atpenins, potent and specific inhibitors of mitochondrial complex II (succinate-ubiquinone oxidoreductase), Proc. Natl. Acad. Sci. U. S. A. 100 (2003) 473–477.
[40] Y. Kido, K. Sakamoto, K. Nakamura, M. Harada, T. Suzuki, Y. Yabu, H. Saimoto, F. Yamakura, D. Ohmori, A. Moore, S. Harada, K. Kita, Purification and kinetic characterization of recombinant alternative oxidase from *Trypanosoma brucei brucei*, Biochim. Biophys. Acta 1797 (2010) 443–450.
[41] B.E. Baysal, R.E. Ferrell, J.E. Willett-Brozick, E.C. Lawrence, D. Myssiorek, A. Bosch, A. van der Mey, P.E. Taschner, W.S. Rubinstein, E.N. Myers, C.W. Richard, C.J. Cornelisse, P. Devilee, B. Devlin, Mutations in SDHD, a mitochondrial complex II gene, in hereditary paraganglioma, Science 287 (2000) 848–851.
[42] G.L. Semenza, Oxygen sensing, homeostasis, and disease, N. Engl. J. Med. 365 (2011) 537–547.
[43] M. Goto, H. Amino, M. Nakajima, N. Tsuji, K. Sakamoto, K. Kita, Cloning and characterization of hypoxia-inducible factor-1 subunits from *Ascaris suum* - a parasitic nematode highly adapted to changes of oxygen conditions during its life cycle, Gene (in press), http://dx.doi.org/10.1016/j.gene.2012.12.025.
[44] E. Tomitsuka, H. Hirawake, Y. Goto, M. Taniwaki, S. Harada, K. Kita, Direct evidence for two distinct forms of the flavoprotein subunit of human mitochondrial complex II (succinate-ubiquinone reductase), J. Biochem. 134 (2003) 191–195.
[45] E. Tomitsuka, Y. Goto, M. Taniwaki, K. Kita, Direct evidence for expression of type II flavoprotein subunit in human complex II (succinate-ubiquinone reductase), Biochem. Biophys. Res. Commun. 311 (2003) 774–779.
[46] T. Bourgeron, P. Rustin, D. Chretien, M. Birch-Machin, M. Bourgeois, E. Viegas-Péquignot, A. Munnich, A. Rötig, Mutation of a nuclear succinate dehydrogenase gene results in mitochondrial respiratory chain deficiency, Nat. Genet. 11 (1995) 144–149.
[47] B.E. Baysal, E.C. Lawrence, R.E. Ferrell, Sequence variation in human succinate dehydrogenase genes: evidence for long-term balancing selection on SDHA, BMC Biol. 5 (2007) 12.
[48] C. Sakai, E. Tomitsuka, H. Esumi, S. Harada, K. Kita, Mitochondrial fumarate reductase as a target of chemotherapy: from parasites to cancer cells, Biochim. Biophys. Acta 1820 (2012) 643–651.
[49] E. Tomitsuka, K. Kita, H. Esumi, An anticancer agent, pyrvinium pamoate inhibits the NADH-fumarate reductase system—a unique mitochondrial energy metabolism in tumour microenvironments, J. Biochem. 152 (2012) 171–183.

Please cite this article as: S. Harada, et al., Diversity of parasite complex II, Biochim. Biophys. Acta (2013), http://dx.doi.org/10.1016/j.bbabio.2013.01.005

Structure of the trypanosome cyanide-insensitive alternative oxidase

Tomoo Shiba[a,1,2], Yasutoshi Kido[a,1,3], Kimitoshi Sakamoto[a,4], Daniel Ken Inaoka[a], Chiaki Tsuge[a], Ryoko Tatsumi[a], Gen Takahashi[b], Emmanuel Oluwadare Balogun[a,b,c], Takeshi Nara[d], Takashi Aoki[d], Teruki Honma[e], Akiko Tanaka[e], Masayuki Inoue[f], Shigeru Matsuoka[f], Hiroyuki Saimoto[g], Anthony L. Moore[h], Shigeharu Harada[b,5], and Kiyoshi Kita[a,5]

[a]Department of Biomedical Chemistry, Graduate School of Medicine, and [f]Graduate School of Pharmaceutical Sciences, The University of Tokyo, Tokyo 113-0033, Japan; [b]Department of Applied Biology, Graduate School of Science and Technology, Kyoto Institute of Technology, Kyoto 606-8585, Japan; [c]Department of Biochemistry, Ahmadu Bello University, Zaria 2222, Nigeria; [d]Department of Molecular and Cellular Parasitology, Juntendo University School of Medicine, Tokyo 113-8421, Japan; [e]Systems and Structural Biology Center, RIKEN, Tsurumi, Yokohama 230-0045, Japan; [g]Department of Chemistry and Biotechnology, Graduate School of Engineering, Tottori University, Tottori 680-8552, Japan; and [h]Biochemistry and Molecular Biology, School of Life Sciences, University of Sussex, Brighton BN1 9QG, United Kingdom

Edited[†] by John E. Walker, Medical Research Council Mitochondrial Biology Unit, Cambridge, United Kingdom, and approved February 11, 2013 (received for review October 23, 2012)

In addition to haem copper oxidases, all higher plants, some algae, yeasts, molds, metazoans, and pathogenic microorganisms such as *Trypanosoma brucei* contain an additional terminal oxidase, the cyanide-insensitive alternative oxidase (AOX). AOX is a diiron carboxylate protein that catalyzes the four-electron reduction of dioxygen to water by ubiquinol. In *T. brucei*, a parasite that causes human African sleeping sickness, AOX plays a critical role in the survival of the parasite in its bloodstream form. Because AOX is absent from mammals, this protein represents a unique and promising therapeutic target. Despite its bioenergetic and medical importance, however, structural features of any AOX are yet to be elucidated. Here we report crystal structures of the trypanosomal alternative oxidase in the absence and presence of ascofuranone derivatives. All structures reveal that the oxidase is a homodimer with the nonhaem diiron carboxylate active site buried within a four-helix bundle. Unusually, the active site is ligated solely by four glutamate residues in its oxidized inhibitor-free state; however, inhibitor binding induces the ligation of a histidine residue. A highly conserved Tyr220 is within 4 Å of the active site and is critical for catalytic activity. All structures also reveal that there are two hydrophobic cavities per monomer. Both inhibitors bind to one cavity within 4 Å and 5 Å of the active site and Tyr220, respectively. A second cavity interacts with the inhibitor-binding cavity at the diiron center. We suggest that both cavities bind ubiquinol and along with Tyr220 are required for the catalytic cycle for O_2 reduction.

diiron protein | neglected tropical diseases | monotopic membrane protein | drug target | ubiquinol oxidase

The alternative oxidase (AOX) is a nonprotonmotive ubiquinol oxidase catalyzing the four-electron reduction of dioxygen to water (1). The gene encoding this protein has been found in all higher plants, some algae, yeast, slime molds, free-living amoebae, eubacteria, nematodes, and some parasites including *Trypanosoma brucei* (2–5). *T. brucei* is a parasite that causes human African sleeping sickness and nagana in livestock and is transmitted by the tsetse fly (5). The development of chemotherapy and the continued search for new, unique therapeutic targets for African trypanosomiasis are urgently required, because current treatments, which are poorly targeted, have unacceptable side effects and efficacy (6).

The bloodstream form of *T. brucei* is equipped with a unique energy metabolism, namely an altered respiratory chain (5) and a modified ATP synthase (7). The parasites live as the bloodstream form in the mammalian host and as the procyclic form in the tsetse fly (5). The procyclic form of *T. brucei* contains a cytochrome-dependent respiratory chain in addition to an alternative oxidase, whereas within the bloodstream trypanosomes use the glycolytic pathway, localized in the glycosome, as their major source of ATP (5, 8). Once the parasites invade the mammalian host in the bloodstream, both the cytochrome respiratory pathway and oxidative phosphorylation disappear and are replaced by the trypanosomal alternative oxidase (TAO), which functions as the sole terminal oxidase to reoxidize NADH accumulated during glycolysis (5). Because NADH reoxidation is essential for parasite survival and mammalian hosts do not possess this protein, TAO is considered to be a unique target for antitrypanosomal drugs (9). Indeed, we have previously reported that the antibiotic ascofuranone (AF), isolated from the pathogenic fungus *Ascochyta viciae*, specifically inhibits the quinol oxidase activity of TAO at subnanomolar concentrations and rapidly kills the parasites (10). Furthermore, we have confirmed the chemotherapeutic efficacy of ascofuranone in vivo (11, 12).

Despite universal conservation of the gene encoding the AOX and diversified physiology (2), the molecular features of this protein have yet to be fully characterized. Current structural models predict that the AOX is an integral interfacial membrane protein that interacts with a single leaflet of the lipid bilayer and contains a nonhaem diiron carboxylate active site (1, 13, 14). This model is supported by extensive site-directed mutagenesis and spectroscopic studies (3, 15–20).

There are many proteins that belong to the diiron carboxylate protein family, and in each case they are characterized by the possession of two copies of the diiron binding motifs (21, 22). To date the majority of proteins within this family whose crystal structures have been determined are soluble proteins, and hence determination of a crystal structure of a member of the membrane-bound class is vital, because it would transformationally improve our understanding of the structure–function relationships of this functionally diverse family of proteins. In this paper we report on the crystal structure of the

Author contributions: T.S., Y.K., K.S., D.K.I., E.O.B., A.L.M., S.H., and K.K. designed research; T.S., Y.K., D.K.I., C.T., R.T., G.T., E.O.B., and H.S. performed research; K.S. and H.S. contributed new reagents/analytic tools; T.S., Y.K., G.T., T.N., T.A., T.H., A.T., M.I., and S.M. analyzed data; and T.S., Y.K., A.L.M., S.H., and K.K. wrote the paper.

The authors declare no conflict of interest.

[†]This Direct Submission article had a prearranged editor.

Data deposition: The atomic coordinates and structure factors have been deposited in the Protein Data Bank, www.pdb.org (PDB ID codes 3VV9 [trypanosomal alternative oxidase (TAO)], 3VVA [TAO-AF2779OH complex], and 3W54 [TAO-colletochlorin B complex]).

[1]T.S. and Y.K. contributed equally to this work.

[2]Present address: Department of Applied Biology, Graduate School of Science and Technology, Kyoto Institute of Technology, Kyoto 606-8585, Japan.

[3]Present address: Division of International Health, Oita University Faculty of Medicine, Yufu, Oita 879-5593, Japan.

[4]Present address: Faculty of Agriculture and Life Science, Hirosaki University, Hirosaki 036-8561, Japan.

[5]To whom correspondence may be addressed. E-mail: harada@kit.ac.jp or kitak@m.u-tokyo.ac.jp.

This article contains supporting information online at www.pnas.org/lookup/suppl/doi:10.1073/pnas.1218386110/-/DCSupplemental.

oxidized form of the trypanosomal alternative oxidase at 2.85 Å. In addition to this very important milestone we also describe the structures of the active site of the enzyme in the presence of AF derivatives, AF2779OH and colletochlorin B (CCB), at 2.6 Å and 2.3 Å resolution, respectively. We believe that a detailed knowledge of the active site of the enzyme in the presence of such inhibitors will lead to a greater rational design of further potent and safer antitrypanosomal drugs.

Results and Discussion

Overall Structure of TAO. We have recently established protocols to prepare highly purified and stable TAO, which has enabled us to crystallize the enzyme (23, 24). The crystal structure of TAO determined at 2.85 Å resolution (*SI Appendix*, Table S1) contains four monomers per asymmetric unit that associate to form homodimers (Fig. 1*A* and *SI Appendix*, Fig. S1*A*). Each monomer, which lacks about 30 residues in both N- and C-terminal regions due to faint electron density, consists of a long N-terminal arm, six long α helices (α1–α6), and four short helices (S1–S4). The long helices are arranged in an antiparallel fashion with α2, α3, α5, and α6 forming a four-helix bundle that accommodates a diiron center, as widely observed in other diiron carboxylate proteins (1, 14) (*SI Appendix*, Fig. S2). Except for the N-terminal arm, each monomer is shaped as a compact cylinder (50 × 35 × 30 Å), and there are no significant structural differences among monomers in the asymmetric unit, as indicated by rms deviations (0.49~0.68 Å) for superimposed Cα positions of the six helices calculated between a pair of monomers. However, loops connecting adjacent helices show larger differences among monomers, resulting in somewhat larger rms deviations (0.67~0.88 Å) when calculated using all Cα atoms.

In the dimer, two monomers are related by a noncrystallographic twofold axis approximately perpendicular to the bundle (Fig. 1*A*). Helices α2, α3, and α4 of one monomer and α2*, α3*, and α4* of the other (asterisk denotes helix of a neighboring monomer) build a dimer interface, where six completely conserved residues (H138, L142, R143, R163, L166, and Q187) and 12 highly conserved residues (M131, M135, L139, S141, M145, R147, D148, L156, A159, M167, R180, and I183) are involved in the interaction between monomers (*SI Appendix*, Fig. S3), suggesting that a dimeric structure is common to all AOXs. In addition, the N-terminal arm (P31~R62) of one monomer extends into the other monomer (Fig. 1*A*), suggesting that the arm is important for dimerization. Upon dimerization, about 2,490 Å^2 of solvent-accessible surface (35% of the total dimer surface) is buried. A large hydrophobic region is visible on one side of the dimer surface that is formed by α1 and α4 plus the C-terminal region of α2 and the N-terminal region of α5 from both monomers (Fig. 1*B Left*). Because the opposite side of the dimer surface is relatively hydrophilic (Fig. 1*B Right*), we propose that the dimer is bound to the mitochondrial inner membrane via this hydrophobic region in an interfacial fashion, as originally suggested by Andersson and Nordlund (13). The membrane penetration depth of TAO, calculated by PPM web server (25), is 8.4 Å, roughly corresponding to the radius of a helix. In addition, basic residues (R106, R143, R180, R203, and R207) are distributed along a boundary between the hydrophobic and hydrophilic regions of the dimer surface (Fig. 1*C* and *SI Appendix*, Fig. S4). They are conserved across all amino acid sequences of the membrane-bound AOXs shown in *SI Appendix*, Fig. S5, and their locations make these residues ideal candidates to interact with the negatively charged phospholipids head groups of membranes.

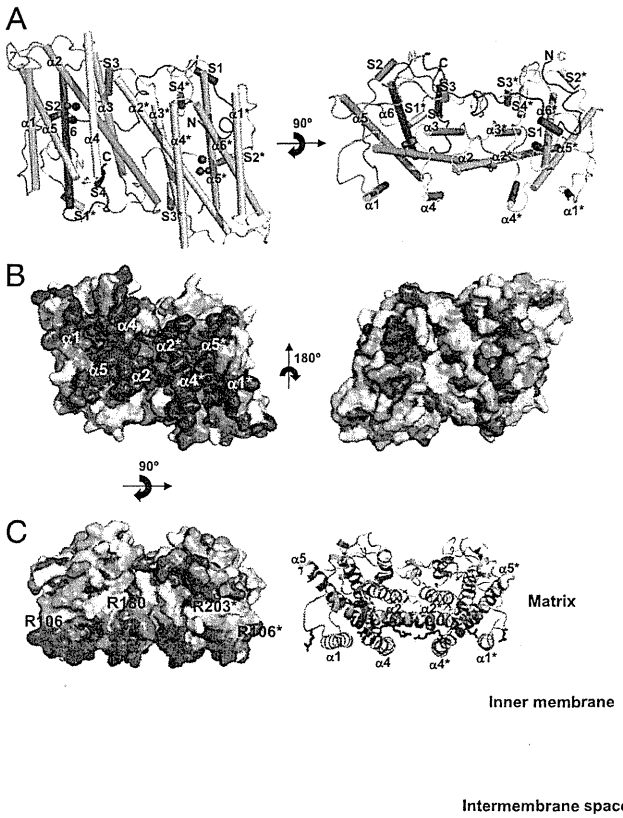

Fig. 1. Structure of TAO. Long helices are labeled α1 to α6 and short ones S1 to S4. Diiron and hydroxo atoms are shown as magenta spheres. (*A*) Dimeric structure of TAO viewed roughly perpendicular (*Left*) and parallel (*Right*) to the helix axes. Helices are shown as cylinders. Chain A is colored in rainbow from blue (N terminus) to red (C terminus) and chain B in pink. (*B*) Surface representation of the TAO dimer showing the hydrophobic (*Left*) and hydrophilic (*Right*) surfaces. Colors are according to the following hydrophobicity scale: red, high hydrophobicity; white, low hydrophobicity (www.pymolwiki.org/index.php/Color_h). (*C*) Proposed binding model of the TAO dimer to membranes shown by surface (*Left*) and cartoon (*Right*) representations. The hydrophobic region on the molecular surface of the TAO dimer faces the membrane. Conserved basic amino acid residues, which are distributed along a boundary between the hydrophobic and hydrophilic regions of the dimer surface, are colored in blue. Residue names are labeled in black (asterisk denotes in chain B).

Structure of Diiron Active Site. The structure of the diiron active site was refined as an oxidized Fe(III)-Fe(III) form with a single hydroxo-bridge (Fig. 2 and *SI Appendix*, Fig. S6), as previously predicted from spectroscopic studies (19, 20). The active site, which is located in a hydrophobic environment deep inside the TAO molecule, is composed of the diiron center and four glutamate (E123, E162, E213, and E266) and two histidine residues (H165 and H269), all of which are completely conserved (*SI Appendix*, Fig. S5). In addition, the conserved hydrophobic residues (L122, A126, L212, A216, Y220, and I262) are within 6 Å of the diiron center (Fig. 2*A*). The average Fe1–Fe2 distance of the four monomers in the asymmetric unit is 3.3 ± 0.2 Å and, in addition to the hydroxo-bridge, Fe1 and Fe2 are bridged by E162 and E266 and furthermore coordinated in a bidentate fashion by E123 and E213, respectively, thereby resulting in a five-coordinated diiron center possessing a distorted square pyramidal geometry (Fig. 2*B* and *SI Appendix*, Fig. S6 and Table S2). The most striking feature of the diiron active site in the oxidized state is that, as predicted from our earlier FTIR studies (26), histidine residues (H165 and H269) are too distant from both Fe1 and Fe2 (H165: 3.3~4.0 Å, H269: 3.8~4.4 Å) to coordinate to the diiron center. They do, however, form hydrogen bonds with E123, N161, E162, E213, and D265. N161 and D265 are situated in the center of the hydrogen-bond network and extend the network to W65, Y246, and W247. These residues, apart from W65, are again completely conserved (*SI Appendix*, Fig. S5), suggesting that the hydrogen bond network is important for the stabilization of the AOX active site. To our knowledge, TAO is the only structure of